The current issue and full text archive of this journal is available at
www.emeraldinsight.com/0264-4401.htm

Higher-order linked interpolation in triangular thick plate finite elements

Dragan Ribarić and Gordan Jelenić
Faculty of Civil Engineering, University of Rijeka, Rijeka, Republic of Croatia

Received 20 March 2012
Revised 30 August 2012
27 September 2012
Accepted 3 October 2012

Abstract

Purpose – In this work, the authors aim to employ the so-called linked-interpolation concept already tested on beam and quadrilateral plate finite elements in the design of displacement-based higher-order triangular plate finite elements and test their performance.

Design/methodology/approach – Starting from the analogy between the Timoshenko beam theory and the Mindlin plate theory, a family of triangular linked-interpolation plate finite elements of arbitrary order are designed. The elements are tested on the standard set of examples.

Findings – The derived elements pass the standard patch tests and also the higher-order patch tests of an order directly related to the order of the element. The lowest-order member of the family of developed elements still suffers from shear locking for very coarse meshes, but the higher-order elements turn out to be successful when compared to the elements from literature for the problems with the same total number of the degrees of freedom.

Research limitations/implications – The elements designed perform well for a number of standard benchmark tests, but the well-known Morley's skewed plate example turns out to be rather demanding, i.e. the proposed design principle cannot compete with the mixed-type approach for this test. Work is under way to improve the proposed displacement-based elements by adding a number of internal bubble functions in the displacement and rotation fields, specifically chosen to satisfy the basic patch test and enable a softer response in the bench-mark test examples.

Originality/value – A new family of displacement-based higher-order triangular Mindlin plate finite elements has been derived. The higher-order elements perform very well, whereas the lowest-order element requires improvement.

Keywords Higher-order linked interpolation, Mindlin plate theory, Triangular plate finite elements

Paper type Research paper

1. Introduction

Owing to its close relationship with the Timoshenko theory of thick beams, the idea of linking the displacement field to the rotations of the cross-sections has been often studied and thoroughly investigated and exploited in finite-element applications of the Mindlin moderately thick plate theory (Auricchio and Taylor, 1993, 1994; Ibrahimbegović, 1993; Chinosi and Lovadina, 1995; Auricchio and Lovadina, 2001; Taylor and Govindjee, 2002; Zienkiewicz and Taylor, 2005; Liu and Riggs, 2005; de Miranda and Ubertini, 2006; Crisfield, 1986; Zienkiewicz *et al.*, 1993; Taylor and Auricchio, 1993; Xu *et al.*, 1994; Chen and Cheung, 2000, 2001, 2005). It has been found out that the idea on its own cannot eliminate the problem of shear locking even though this result may be achieved for the Timoshenko beam elements (Zienkiewicz and

The results shown here have been obtained within the scientific Project No. 114-0000000-3025: "Improved accuracy in non-linear beam elements with finite 3D rotations" financially supported by the Ministry of Science, Education and Sports of the Republic of Croatia.

Engineering Computations: International Journal for Computer-Aided Engineering and Software
Vol. 31 No. 1, 2014
pp. 69-109

0264-4401
DOI 10.1108/EC-03-2012-0056

Taylor, 2005; Tessler and Dong, 1981; Jelenić and Papa, 2011; Przemieniecki, 1968; Rakowski, 1990; Yunhua, 1998; Reddy, 1997; Mukherjee *et al.*, 2001). Different improvements have been proposed by different authors, which involve adjusted material parameters (Tessler and Hughes, 1985) or the assumed or enhanced strain concepts (Ibrahimbegović, 1993; Chen and Cheung, 2000, 2001; Simo and Rifai, 1990; Bathe *et al.*, 1989; Lee and Bathe, 2004; Kim and Bathe, 2009) or are based on the use of mixed and hybrid approaches (Auricchio and Taylor, 1993, 1994; Taylor and Govindjee, 2002; de Miranda and Ubertini, 2006; Zienkiewicz *et al.*, 1993; Taylor and Auricchio, 1993).

In this paper, we build on the ideas given in Ribarić and Jelenić (2012) where we have re-visited this classic topic and, remaining firmly in the framework of the standard displacement-based design technique, derived a family of quadrilateral thick plate elements by extending higher-order linked interpolation functions developed for the Timoshenko beams. Here, we apply the methodology to the popular class of triangular elements and contrast it to an alternative methodology of devising higher-order linked interpolation for this class of elements (Liu and Riggs, 2005).

In Section 2, we present the family of interpolation functions for the Timoshenko beam elements which provide the exact solution for arbitrary polynomial loadings (Jelenić and Papa, 2011). Even though the Mindlin theory of thick plates may be regarded as a 2D generalisation of the Timoshenko theory of thick beams, the differential equations of equilibrium for thick plates cannot be solved in terms of a finite number of parameters and so, in contrast to beams, there does not exist an exact finite-element interpolation. Nonetheless, in Auricchio and Taylor (1993, 1994, 1995) such interpolation has been used to formulate three-node triangular and four-node quadrilateral thick plate elements, while in Ibrahimbegović (1993) and Taylor and Govindjee (2002) a six-node triangular and an eight-node quadrilateral elements have been proposed. A family of triangular elements designed in this way has been proposed in Liu and Riggs (2005).

In Section 3, we outline the Mindlin plate theory and continue by considering a triangular three-node element, for which the constant shear strain condition imposed on the element edges is known to lead to an interpolation for the displacement field which is dependent not only on the nodal displacements, but also on the nodal rotations around the in-plane normal directions to the element edges. The same result may be obtained by generalising the linked interpolation for beams (Jelenić and Papa, 2011) to 2D situations. This approach enables a straightforward generalisation of the linked-interpolation beam concept to higher-order triangular plate elements leading to additional internal degrees of freedom which do not exist in the beam elements. A similar goal may be achieved following the approach presented in Liu and Riggs (2005) where a family of displacement-based linked-interpolation triangular elements has been derived by prescribing the order of the shear distribution over the element which, in contrast, does not involve internal degrees of freedom. Generalising either of these ideas to arbitrary curvilinear triangular shapes (on higher-order elements) is non-trivial and special care needs to be taken for such elements to satisfy the standard patch tests.

In Section 4, we compare the two approaches and in Section 5 summarise the finite-element results. Finally, in Section 6 we conduct numerical tests and in Section 7 draw the conclusions.

2. Solution of the Timoshenko beam problem for polynomial loading using linked interpolation of appropriate order

In contrast to the Bernoulli beam theory, in the Timoshenko beam theory the cross section of a beam remains planar after the deformation, but not necessarily orthogonal to the beam centroidal axis. This departure from orthogonality is the shear angle:

$$\gamma = \frac{dw}{dx} + \theta = w' + \theta$$

where w is the lateral displacement of the beam shown in Figure 1, the dash ($'$) indicates a differentiation with respect to the co-ordinate x, and θ is the rotation of a cross section.

Let, the cross-sectional stress-couple and shear stress resultants M and S be linearly dependent on curvature (change of cross-sectional rotation) and shear angle via $M = EI\theta'$ and $S = GA_s\gamma$, where EI and GA_s are the bending and shear stiffness, respectively. As the equilibrium equations are $M' = S$ and $S' = -q$, where q is the distributed loading per unit of length of the beam, this results in the following differential equations:

$$EI\theta''' = -q, \quad GA_s(w'' + \theta') = -q,$$

with the following closed-form solution for a polynomial loading q of order $n - 4$ (Jelenić and Papa, 2011):

$$\theta = \sum_{i=1}^{n} I_i\theta_i, \quad w = \sum_{i=1}^{n} I_i w_i - \frac{L}{n}\prod_{j=1}^{n} N_j \sum_{i=1}^{n} (-1)^{i-1}\binom{n-1}{i-1}\theta_i, \tag{1}$$

where L is the beam length, θ_i and w_i are the values of the displacements and the rotations at the n nodes equidistantly spaced between the beam ends, I_i are the

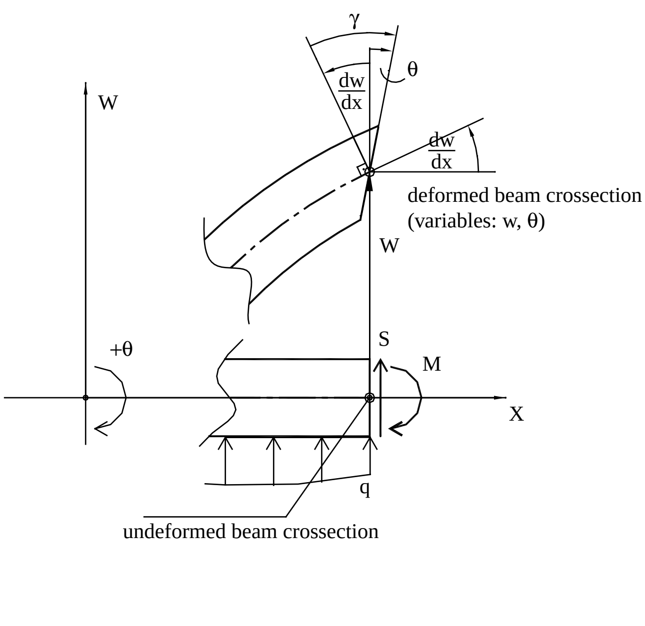

Figure 1.
Initial and deformed configuration of a moderately thick beam

standard Lagrangian polynomials of order $n-1$, and $N_j = x/L$ for $j = 1$ and $N_j = 1 - ((n-1)/(j-1))(x/L)$ otherwise. In the natural co-ordinate system with $\xi = (2x/L) - 1$ the displacement solution reads:

$$w = \sum_{i=1}^{n} I_i w_i - \frac{L}{n} \sum_{i=1}^{n} \frac{\xi - \xi_i}{2} I_i \theta_i.$$

3. Overview of the Mindlin plate theory and a family of triangular linked-interpolation elements

The Mindlin plate theory is closely related to the Timoshenko beam theory and may be regarded as its generalisation to two-dimensional problems. The plate is assumed to be of a uniform thickness h with a mid-surface lying in the horizontal co-ordinate plane and a distributed loading q assumed to act on the plate mid-surface in the direction perpendicular to it. The changes of the angles which the vertical fibres close with the mid-surface are the shear angles:

$$\mathbf{\Gamma} = \begin{Bmatrix} \gamma_{xz} \\ \gamma_{yz} \end{Bmatrix} = \begin{Bmatrix} \theta_y + \frac{\partial w}{\partial x} \\ -\theta_x + \frac{\partial w}{\partial y} \end{Bmatrix} = \begin{bmatrix} 0 & 1 \\ -1 & 0 \end{bmatrix} \begin{Bmatrix} \theta_x \\ \theta_y \end{Bmatrix} + \begin{Bmatrix} \frac{\partial}{\partial x} \\ \frac{\partial}{\partial y} \end{Bmatrix} w = \mathbf{e}\boldsymbol{\theta} + \nabla w \qquad (2)$$

while the curvatures (the fibre's changes of rotations) are:

$$\boldsymbol{\kappa} = \begin{Bmatrix} \kappa_x \\ \kappa_y \\ \kappa_{xy} \end{Bmatrix} = \begin{Bmatrix} \frac{\partial \theta_y}{\partial x} \\ -\frac{\partial \theta_x}{\partial y} \\ \frac{\partial \theta_y}{\partial y} - \frac{\partial \theta_x}{\partial x} \end{Bmatrix} = \begin{bmatrix} 0 & \frac{\partial}{\partial x} \\ -\frac{\partial}{\partial y} & 0 \\ -\frac{\partial}{\partial x} & \frac{\partial}{\partial y} \end{bmatrix} \begin{Bmatrix} \theta_x \\ \theta_y \end{Bmatrix} = \mathbf{L}\boldsymbol{\theta} \qquad (3)$$

where $\boldsymbol{\theta}$ is the rotation vector with components θ_x and θ_y around the respective horizontal global co-ordinate axes, w is the transverse displacement field, $\mathbf{\Gamma}$ is the shear strain vector and $\boldsymbol{\kappa}$ is the curvature vector, ∇w is a gradient on the displacement field and $\mathbf{L}$ is a differential operator on the rotation field (Auricchio and Taylor, 1994). Let us consider a linear elastic material with:

$$\mathbf{M} = \begin{Bmatrix} M_x \\ M_y \\ M_{xy} \end{Bmatrix} = \frac{Eh^3}{12(1-\nu^2)} \begin{bmatrix} 1 & \nu & 0 \\ \nu & 1 & 0 \\ 0 & 0 & \frac{1-\nu}{2} \end{bmatrix} \begin{Bmatrix} \frac{\partial \theta_y}{\partial x} \\ -\frac{\partial \theta_x}{\partial y} \\ \frac{\partial \theta_y}{\partial y} - \frac{\partial \theta_x}{\partial x} \end{Bmatrix} = \mathbf{D_b}\boldsymbol{\kappa} = \mathbf{D_b}\mathbf{L}\boldsymbol{\theta} \qquad (4)$$

$$\mathbf{S} = \begin{Bmatrix} S_x \\ S_y \end{Bmatrix} = kGh \begin{bmatrix} 1 & 0 \\ 0 & 1 \end{bmatrix} \begin{Bmatrix} \gamma_{xz} \\ \gamma_{yz} \end{Bmatrix} = \mathbf{D_s}\mathbf{\Gamma} = \mathbf{D_s}(\mathbf{e}\boldsymbol{\theta} + \nabla w),$$

where M_x, M_y, and M_{xy} are the bending and twisting moments around the respective co-ordinate axes, S_x and S_y are the shear-stress resultants, E and G are the Young and shear moduli, while ν and k are Poisson's coefficient and the shear correction factor usually set to 5/6. The differential equations of equilibrium are:

$$\frac{\partial M_x}{\partial x} + \frac{\partial M_{xy}}{\partial y} = S_x, \quad \frac{\partial M_{xy}}{\partial x} + \frac{\partial M_y}{\partial y} = S_y, \quad \frac{\partial S_x}{\partial x} + \frac{\partial S_y}{\partial y} = -q. \tag{5}$$

Substituting equation (4) in equation (5), results in the differential equations which now cannot be solved in terms of a finite number of parameters as before. Still, we shall attempt to extend the results from Section 2 in order to derive more accurate Mindlin plate elements. To do so, we shall need the functional of the total potential energy:

$$\begin{aligned}\Pi(w, \theta_x, \theta_y) &= \frac{1}{2}\int(\mathbf{M}^T\boldsymbol{\kappa})dA + \frac{1}{2}\int(\mathbf{S}^T\boldsymbol{\Gamma})dA + \Pi_{ext} \\ &= \frac{1}{2}\int(\boldsymbol{\kappa}^T\mathbf{D_b}\boldsymbol{\kappa})dA + \frac{1}{2}\int(\boldsymbol{\Gamma}^T\mathbf{D_s}\boldsymbol{\Gamma})dA + \Pi_{ext},\end{aligned} \tag{6}$$

where the last term describes the potential energy of the distributed and boundary loading.

3.1 Linked interpolation for a three-node triangular plate element

We shall first apply the result given in equation (1) to a triangular element with three nodal points at the element vertices as in Liu and Riggs (2005), Taylor and Auricchio (1993), Chen and Cheung (2001), Tessler and Hughes (1985), Auricchio and Taylor (1995) and Zhu (1992) (Figure 2). The displacements and rotations are expressed in the so-called area coordinates which, for any interior point, make the ratio of the respective interior area to the area of the whole triangle 1-2-3 as shown in Figure 2.

Because in two dimensions any point is uniquely defined by only two coordinates, the three coordinates, ξ_1, ξ_2 and ξ_3 are not independent of each other and for any point within the domain they are related by the expression:

$$\xi_1 + \xi_2 + \xi_3 = 1.$$

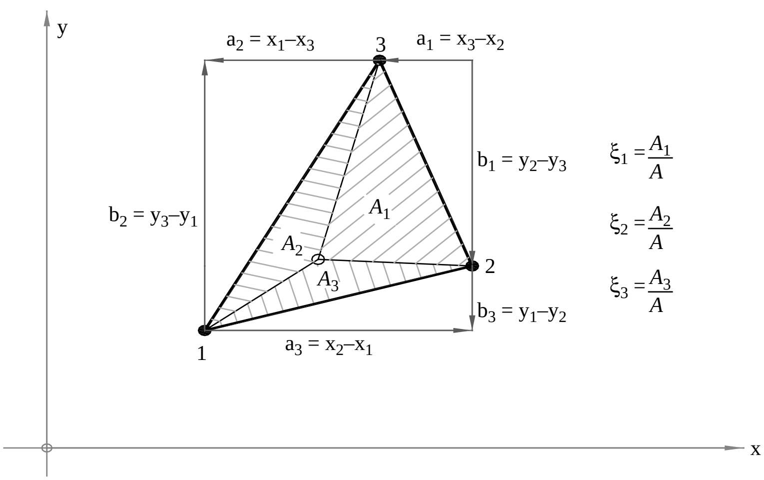

Figure 2.
Three-node triangular plate element and its area coordinates of an interior point

The area coordinates of any point within the domain are transformed into the Cartesian coordinates as:

$$x = \xi_1 x_1 + \xi_2 x_2 + \xi_3 x_3$$

$$y = \xi_1 y_1 + \xi_2 y_2 + \xi_3 y_3$$

and vice versa:

$$\xi_1 = \frac{(x - x_3)b_1 + (y - y_3)a_1}{a_2 b_1 - a_1 b_2} = \frac{2A_1}{2A} = \frac{A_1}{A}$$

$$\xi_2 = \frac{(x - x_1)b_2 + (y - y_1)a_2}{a_3 b_2 - a_2 b_3} = \frac{A_2}{A}$$

$$\xi_3 = \frac{(x - x_2)b_3 + (y - y_2)a_3}{a_1 b_3 - a_3 b_1} = \frac{A_3}{A},$$

where $a_i = x_k - x_j$ and $b_i = y_j - y_k$ are the directed side-length projections along the coordinate axes and the indices i, j, and k denoting the triangle vertices are cyclic permutations of 1, 2 and 3. The area $A_i = (1/2)[(x - x_k)b_i - (y_k - y)a_i]$ denotes the area of the interior triangle whose one vertex is at the point (x, y) while the other two are the vertices j and k, while $A = (1/2)(a_j b_i - a_i b_j)$ is the area of the whole triangle (Figure 2). Note that the area co-ordinates ξ_1, ξ_2, ξ_3 are in fact the standard linear Lagrangian shape functions over a triangular domain.

If any triangle side k of length s_k (where $s_k^2 = a_k^2 + b_k^2$) is taken as a beam element (Figure 3), the expressions for the displacement w and the rotation around the in-plane normal θ_n can be derived in linked form (1):

$$\begin{aligned} w &= \xi_i w_i + \xi_j w_j - \xi_i \xi_j \frac{s_k}{2}(\theta_{ni} - \theta_{nj}) \\ &= \xi_i w_i + \xi_j w_j - \xi_i \xi_j \frac{s_k}{2}[(\theta_{yi} - \theta_{yj})\cos\alpha_k - (\theta_{xi} - \theta_{xj})\sin\alpha_k] \\ &= \xi_i w_i + \xi_j w_j - \frac{1}{2}\,\xi_i \xi_j[(\theta_{xi} - \theta_{xj})b_k + (\theta_{yi} - \theta_{yj})a_k], \\ \theta_n &= \xi_i \theta_{ni} + \xi_j \theta_{nj}, \end{aligned}$$

while $\xi_k = 0$. Such interpolation provides constant moments and constant shear along the element side.

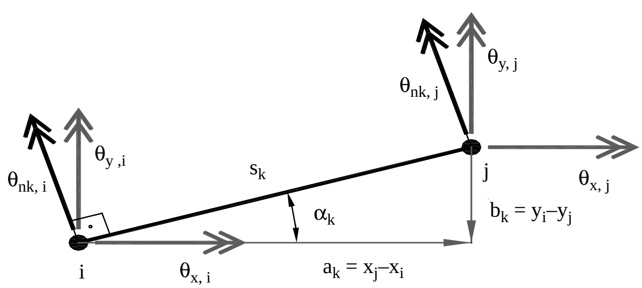

Figure 3.
Triangular element's side and its rotation degrees of freedom

At each nodal point i ($i = 1, 2, 3$) of an element there exist three degrees of freedom (displacement w_i, and rotations θ_{xi}, and θ_{yi} in the global coordinate directions). The linked interpolation for the displacement and rotation field over the whole triangular domain may be now proposed as:

$$\begin{aligned} w = {} & \xi_1 w_1 + \xi_2 w_2 + \xi_3 w_3 - \frac{1}{2}\,\xi_1\xi_2[(\theta_{x1} - \theta_{x2})b_3 + (\theta_{y1} - \theta_{y2})a_3] \\ & - \frac{1}{2}\,\xi_2\xi_3[(\theta_{x2} - \theta_{x3})b_1 + (\theta_{y2} - \theta_{y3})a_1] \\ & - \frac{1}{2}\,\xi_3\xi_1[(\theta_{x3} - \theta_{x1})b_2 + (\theta_{y3} - \theta_{y1})a_2] \end{aligned} \tag{7}$$

$$\theta_x = \xi_1\theta_{x1} + \xi_2\theta_{x2} + \xi_3\theta_{x3} \tag{8}$$

$$\theta_y = \xi_1\theta_{y1} + \xi_2\theta_{y2} + \xi_3\theta_{y3}. \tag{9}$$

Here, θ_{xi}, θ_{yi} are the rotation components at the element vertices (Figure 4). Terms in brackets are rotational projections of respective rotation components to the normal on each element side times the side length. Therefore, the interpolation is isoparametric for the rotations, while for the displacement function it includes an additional linking part schematically presented in Figure 5:

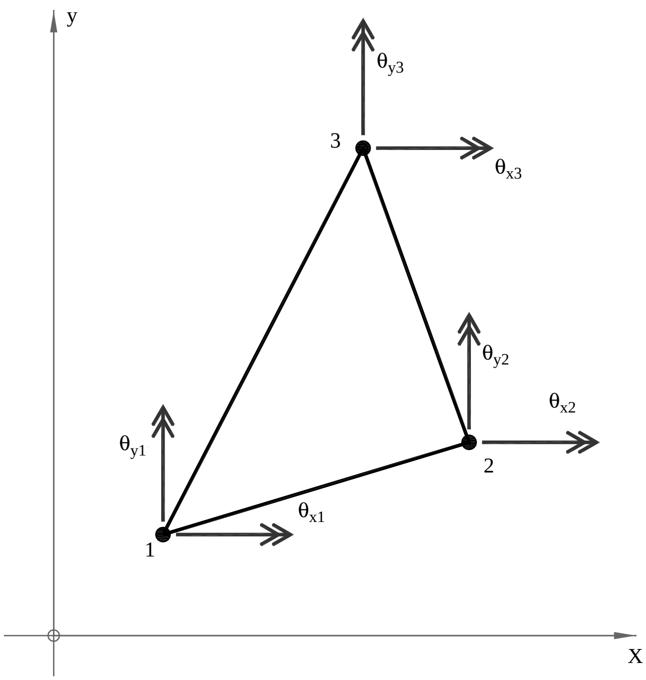

Note: The nodal displacements are perpendicular to the element plane

Figure 4. Three-node triangular plate element and its nodal rotations

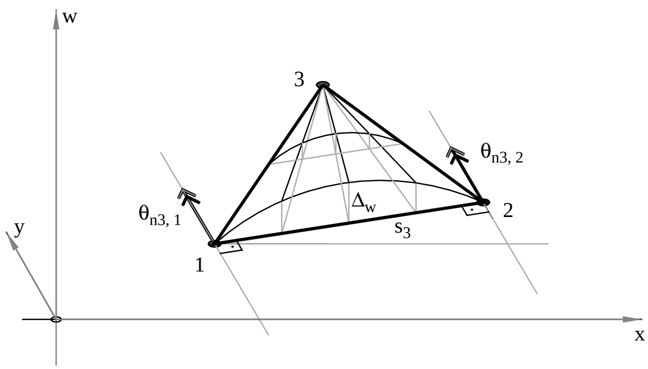

Figure 5.
Linking part of the shape function on side "1-2" of the element

$$\Delta w = -\frac{1}{2}\,\xi_1\xi_2[(\theta_{x1} - \theta_{x2})b_3 + (\theta_{y1} - \theta_{y2})a_3]$$

The linked interpolation as employed in a two-node Timoshenko beam element can exactly reproduce the quadratic displacement function, and the same should be expected for the 2D interpolation considered here. The finite element developed on this basis will be named *T3-U2*, denoting the three-node element with the second-order displacement distribution.

3.2 Linked interpolation for a six-node triangular plate element

A six-node linked-interpolation triangular element (Figure 6) may be defined correspondingly.

Again, if any triangle side k is taken as a beam element, the expressions for the displacement w and the rotation around the in-plane normal θ_n can be derived in the linked form (1), with $i+3$ node located at the middle of the side as in Figure 7:

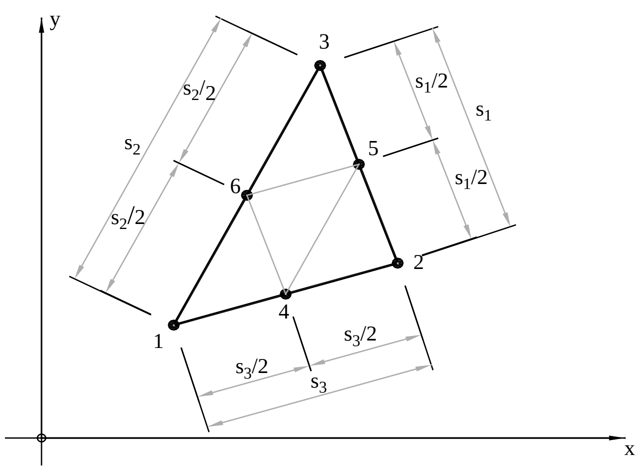

Figure 6.
Six-node triangular plate element and its geometry

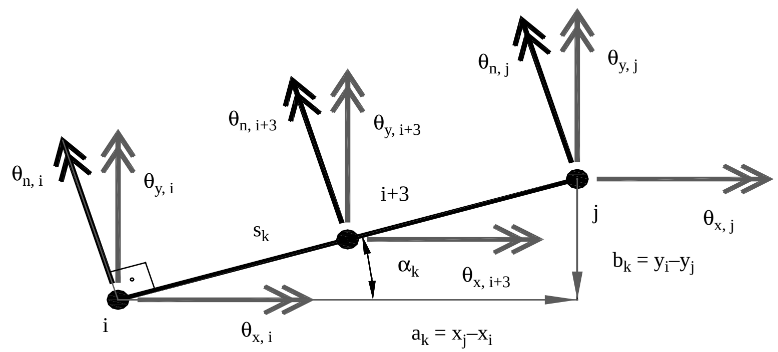

Figure 7. Triangular element's side and its rotation degrees of freedom

$$
\begin{aligned}
w &= \xi_i(2\xi_i-1)w_i+\xi_j(2\xi_j-1)w_j+4\xi_i\xi_j w_{i+3}-\xi_i\xi_j(\xi_j-\xi_i)\frac{s_k}{3}(-\theta_{n,i}+2\theta_{n,i+3}-\theta_{n,j})\\
&=\xi_i(2\xi_i-1)w_i+\xi_j(2\xi_j-1)w_j+4\xi_i\xi_j w_{i+3}-\xi_i\xi_j(\xi_j-\xi_i)\frac{1}{3}[(-\theta_{xi}+2\theta_{x,i+3}-\theta_{xj})b_k\\
&\quad+(-\theta_{yi}+2\theta_{y,i+3}-\theta_{yj})a_k]\theta_n=\xi_i(2\xi_i-1)\theta_{n,i}+\xi_j(2\xi_j-1)\theta_{n,j}+4\xi_i\xi_j\theta_{n,i+3},
\end{aligned}
$$

since $\xi_k=0$.

Such interpolation may describe a linear moment and shear change along the element side.

The linked interpolation for the displacement field over the whole triangle domain may be now given as:

$$
\begin{aligned}
w^* &= \xi_1(2\xi_1-1)w_1+\xi_2(2\xi_2-1)w_2+\xi_3(2\xi_3-1)w_3+4\xi_1\xi_2w_4+4\xi_2\xi_3w_5\\
&\quad+4\xi_3\xi_1w_6-\xi_1\xi_2(\xi_2-\xi_1)\frac{1}{3}[(-\theta_{x1}+2\theta_{x4}-\theta_{x2})b_3+(-\theta_{y1}+2\theta_{y4}-\theta_{y2})a_3]\\
&\quad-\xi_2\xi_3(\xi_3-\xi_2)\frac{1}{3}[(-\theta_{x2}+2\theta_{x5}-\theta_{x3})b_1+(-\theta_{y2}+2\theta_{y5}-\theta_{y3})a_1]\\
&\quad-\xi_3\xi_1(\xi_1-\xi_3)\frac{1}{3}[(-\theta_{x3}+2\theta_{x6}-\theta_{x1})b_2+(-\theta_{y3}+2\theta_{y6}-\theta_{y1})a_2]
\end{aligned}
\tag{10}
$$

while the interpolation for the rotations takes the standard Lagrangian form:

$$
\begin{aligned}
\theta_x &= \xi_1(2\xi_1-1)\theta_{x1}+\xi_2(2\xi_2-1)\theta_{x2}+\xi_3(2\xi_3-1)\theta_{x3}+4\xi_1\xi_2\theta_{x4}\\
&\quad+4\xi_2\xi_3\theta_{x5}+4\xi_3\xi_1\theta_{x6}
\end{aligned}
\tag{11}
$$

$$
\begin{aligned}
\theta_y &= \xi_1(2\xi_1-1)\theta_{y1}+\xi_2(2\xi_2-1)\theta_{y2}+\xi_3(2\xi_3-1)\theta_{y3}+4\xi_1\xi_2\theta_{y4}\\
&\quad+4\xi_2\xi_3\theta_{y5}+4\xi_3\xi_1\theta_{y6}
\end{aligned}
\tag{12}
$$

where θ_{xi}, θ_{yi} are the nodal rotation components at the element vertices and midpoints. As before, the displacement and rotation fields are interpolated using the same interpolation functions, but the displacement field has an additional linking part expressed in terms of the rotational components on each element side.

The rotations in equations (11) and (12) have a full quadratic polynomial form, but the displacement field does not have a full cubic polynomial form since expression (10) misses the tenth item in Pascal's triangle with the function that has zero values along all the element sides which cannot be associated with any nodal degree of freedom. To provide the full cubic expansion we need to expand the result from equation (10) with an independent bubble degree of freedom w_b i.e:

$$w = w^* + \xi_1 \xi_2 \xi_3 w_b \tag{13}$$

The finite element developed on this basis will be named *T6-U3*, denoting the six-node element with the third-order displacement distribution. The same interpolation for the displacements has been applied to the mixed-type six-node triangular plate element in Taylor and Govindjee (2002).

3.3 Linked interpolation for a ten-node triangular plate element

A ten-node linked-interpolation triangular element (Figure 8) follows analogously from the linked interpolation for the four-node Timoshenko beam element.

Any triangle side can be taken as a beam element and expressions for w and θ_n can be expressed in the linked form (1). Completed over the whole triangle, the interpolations for the displacement and the rotations follow as:

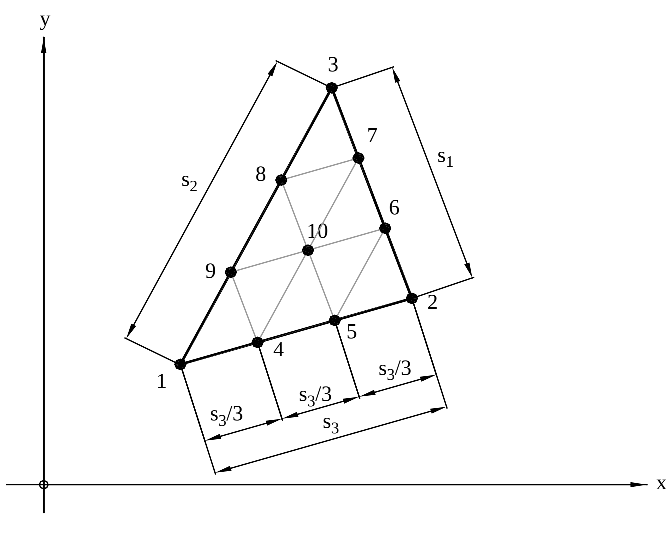

Figure 8.
Ten-node triangular plate element and its geometry

$$
\begin{aligned}
w^{*} &= \xi_1(3\xi_1-2)(3\xi_1-1)\frac{1}{2}w_1+\xi_1\xi_2(3\xi_1-1)\frac{9}{2}w_4+\xi_1\xi_2(3\xi_2-1)\frac{9}{2}w_5 \\
&+\xi_2(3\xi_2-2)(3\xi_2-1)\frac{1}{2}w_2+\xi_2\xi_3(3\xi_2-1)\frac{9}{2}w_6+\xi_2\xi_3(3\xi_3-1)\frac{9}{2}w_7 \\
&+\xi_3(3\xi_3-2)(3\xi_3-1)\frac{1}{2}w_3+\xi_3\xi_1(3\xi_3-1)\frac{9}{2}w_8+\xi_3\xi_1(3\xi_1-1)\frac{9}{2}w_9 \\
&+27\xi_1\xi_2\xi_3w_{10}-\xi_1\xi_2(3\xi_1-1)(3\xi_2-1)\frac{1}{8}[(-\theta_{x1}+3\theta_{x4}-3\theta_{x5}+\theta_{x2})b_3 \\
&+(-\theta_{y1}+3\theta_{y4}-3\theta_{y5}+\theta_{y2})a_3]-\xi_2\xi_3(3\xi_2-1)(3\xi_3-1)\frac{1}{8}[(-\theta_{x2}+3\theta_{x6}-3\theta_{x7}+\theta_{x3})b_1 \\
&+(-\theta_{y2}+3\theta_{y6}-3\theta_{y7}+\theta_{y3})a_1]-\xi_3\xi_1(3\xi_3-1)(3\xi_1-1) \\
&\times\frac{1}{8}[(-\theta_{x3}+3\theta_{x8}-3\theta_{x9}+\theta_{x1})b_2+(-\theta_{y3}+3\theta_{y8}-3\theta_{y9}+\theta_{y1})a_2]
\end{aligned}
\tag{14}
$$

$$
\begin{aligned}
\theta_x &= \xi_1(3\xi_1-2)(3\xi_1-1)\frac{1}{2}\,\theta_{x1}+\xi_1\xi_2(3\xi_1-1)\frac{9}{2}\,\theta_{x4}+\xi_1\xi_2(3\xi_2-1)\frac{9}{2}\,\theta_{x5} \\
&+\xi_2(3\xi_2-2)(3\xi_2-1)\frac{1}{2}\,\theta_{x2}+\xi_2\xi_3(3\xi_2-1)\frac{9}{2}\,\theta_{x6}+\xi_2\xi_3(3\xi_3-1)\frac{9}{2}\,\theta_{x7} \\
&+\xi_3(3\xi_3-2)(3\xi_3-1)\frac{1}{2}\,\theta_{x3}+\xi_3\xi_1(3\xi_3-1)\frac{9}{2}\,\theta_{x8}+\xi_3\xi_1(3\xi_1-1)\frac{9}{2}\,\theta_{x9} \\
&+27\xi_1\xi_2\xi_3\theta_{x10}
\end{aligned}
\tag{15}
$$

$$
\begin{aligned}
\theta_y &= \xi_1(3\xi_1-2)(3\xi_1-1)\frac{1}{2}\,\theta_{y1}+\xi_1\xi_2(3\xi_1-1)\frac{9}{2}\,\theta_{y4}+\xi_1\xi_2(3\xi_2-1)\frac{9}{2}\,\theta_{y5} \\
&+\xi_2(3\xi_2-2)(3\xi_2-1)\frac{1}{2}\,\theta_{y2}+\xi_2\xi_3(3\xi_2-1)\frac{9}{2}\,\theta_{y6}+\xi_2\xi_3(3\xi_3-1)\frac{9}{2}\,\theta_{y7} \\
&+\xi_3(3\xi_3-2)(3\xi_3-1)\frac{1}{2}\,\theta_{y3}+\xi_3\xi_1(3\xi_3-1)\frac{9}{2}\,\theta_{y8}+\xi_3\xi_1(3\xi_1-1)\frac{9}{2}\,\theta_{y9} \\
&+27\xi_1\xi_2\xi_3\theta_{y10}
\end{aligned}
\tag{16}
$$

where θ_{xi}, θ_{yi} are the nodal rotation components at the element vertices and the mid-side points.

The rotations are expressed as a full cubic polynomial, but the displacement field does not have a full quartic polynomial forms. To extend expression (14) to a full quartic form (with all 15 items in Pascal's triangle), two more parameters are needed and they are related with the functions that have zero values along any element side and at the central point (node with index 10). Those parameters are some internal bubbles so finally the displacement field may be completed as:

$$w = w^{*} + \xi_1\xi_2\xi_3(\xi_1-\xi_2)w_{b1} + \xi_1\xi_2\xi_3(\xi_2-\xi_3)w_{b2} \tag{17}$$

The third term that appears to be missing in expression (17) to complete the cyclic triangle symmetry, namely:

$$\xi_1\xi_2\xi_3(\xi_3-\xi_1)w_{b3},$$

is actually linearly dependent on the two other added terms and the tenth term in equation (14). The finite element developed on the basis of this interpolation will be named *T10-U4*, denoting the ten-node element with the fourth-order displacement distribution.

4. Comparison with Liu-Riggs family of purely displacement-based triangular elements

If arbitrary direction s crossing the triangle element is chosen (Figure 9), the shear strain can be expressed in terms of the shear strains along the directions of the co-ordinate axes x and y as:

$$\gamma_s=\gamma_x\cos\alpha+\gamma_y\sin\alpha, \tag{18}$$

where α is the angle between the s-direction and the x-axis.

In the linked interpolation formulation presented in this work, the expression for the shear along an element side is a polynomial which is two orders lower than the displacement interpolation polynomial. This is also valid for any direction parallel to an element side.

Liu and Riggs (2005) have derived the family of triangle elements likewise based purely on displacement interpolations, which eventually, turn out to be of the linked type in the sense that the displacement distribution also depends on the nodal rotations. In contrast to the approach presented here, however, the requirement that the authors set is that the shear strain along arbitrary direction s, and not only those parallel to the element sides, should satisfy the above condition (Figure 9), thus imposing the pth derivative of equation (18) to be zero for arbitrary α, while the displacement interpolation is of the order $p+2$ and the interpolation for the rotations is of the order $p+1$.

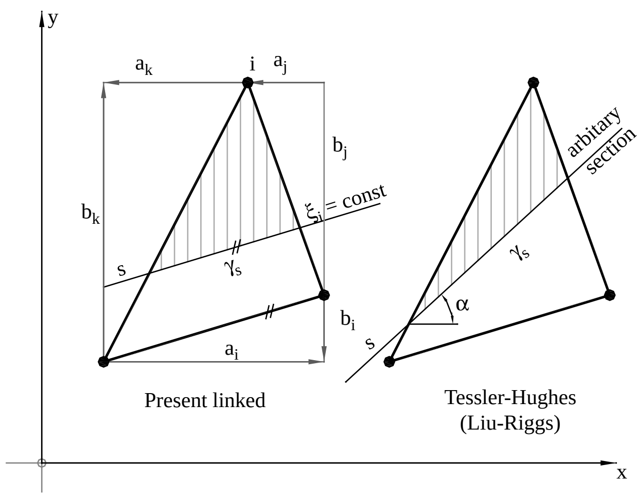

Source: Liu and Riggs (2005)

Figure 9.
Difference in the shear strain condition between the present formulation and the Liu-Riggs formulation

4.1 Liu-Riggs interpolation for a three-node triangular plate element

Liu and Riggs (2005) and Tessler and Hughes (1985) before them, have derived interpolation functions for the triangular element named *MIN3* with three nodes and nine degrees of freedom (the same degrees as the *T3-U2* element presented in Section 3.1) from the condition that the shear strain must be constant along any direction within the element (Tessler and Hughes have additionally introduced a shear-relaxation factor in order to improve the element performance). Their interpolations for the displacement and the rotation fields are:

$$w = N_i w_i + L_i \theta_{xi} + M_i \theta_{yi}, \quad \theta_x = N_i \theta_{xi} \text{ and } \theta_y = N_i \theta_{yi} \tag{19}$$

where the interpolation functions are:

$$N_i = \xi_i, \quad L_i = \frac{1}{2}(b_k \xi_i \xi_j - b_j \xi_k \xi_i) \text{ and } M_i = -\frac{1}{2}(a_j \xi_k \xi_i - a_k \xi_i \xi_j) \tag{20}$$

with i, j and k again being the cyclic permutations of 1, 2 and 3. It can be verified that the rigid body conditions are satisfied because:

$$\sum_{i=1}^{3} N_i = 1, \quad \sum_{i=1}^{3} L_i = 0 \text{ and } \sum_{i=1}^{3} M_i = 0, \tag{21}$$

and it can be also verified by direct calculation that the Liu-Riggs interpolation is the same as the linked interpolation given in Section 3.1. Therefore, for the triangular element with three nodes, in the present formulation the shear strain is also constant in any direction and not only along the directions parallel to the sides of the triangle.

4.2 Liu-Riggs interpolation for a six-node triangular plate element – MIN6

Liu and Riggs (2005) have next derived a family of elements based on upgrading the criteria for the shear strain along an arbitrary direction over the element. The second member of the family is the so-called *MIN6* element with six nodal points. The interpolations are derived to provide linear shear in any direction crossing the element. Interpolations in *MIN6* for the displacement and rotations are again:

$$w = N_i w_i + L_i \theta_{xi} + M_i \theta_{yi}, \quad \theta_x = N_i \cdot \theta_{xi} \text{ and } \theta_y = N_i \cdot \theta_{yi} \quad \text{for } i = 1, 2, \ldots, 6 \tag{22}$$

where the actual interpolation functions are:

$$N_i = \xi_i(2\xi_i - 1), \quad N_{i+3} = 4\xi_i \xi_j \quad \text{for } i = 1, 2, 3 \tag{23a}$$

$$L_i = -\xi_i(2\xi_i - 1)\frac{1}{3}(b_k \xi_j - b_j \xi_k), \quad L_{i+3} = -4\xi_i \xi_j \frac{1}{3}\left[b_j\left(\xi_i - \frac{1}{2}\right) - b_i\left(\xi_j - \frac{1}{2}\right)\right] \tag{23b}$$

and:

$$M_i = -\xi_i(2\xi_i - 1)\frac{1}{3}(a_k\xi_j - a_j\xi_k), \quad M_{i+3} = -4\xi_i\xi_j\frac{1}{3}\left[a_j\left(\xi_i - \frac{1}{2}\right) - a_i\left(\xi_j - \frac{1}{2}\right)\right] \tag{23c}$$

It should be stressed that in the expressions for L_{i+3} and M_{i+3} given here a typographic error in the Liu-Riggs original (Liu and Riggs, 2005) is corrected to satisfy the rigid body conditions:

$$\sum_{i=1}^{6} N_i = 1, \quad \sum_{i=1}^{6} L_i = 0 \text{ and } \sum_{i=1}^{6} M_i = 0. \tag{24}$$

The element based on interpolation (equation (23)) – denoted as *MIN6* – has been coded in the finite-element programme environment FEAP (Zienkiewicz and Taylor, 2005) along with the earlier elements *T3-U2*, *T6-U3* and *T10-U4*. In contrast to *MIN3* (without shear relaxation), which corresponds exactly to the *T3-U2* presented in Section 3.1, the *MIN6* element is different from the *T6-U3* presented in Section 3.2, which has an additional bubble degree of freedom. It can be verified by direct calculation that the Liu–Riggs interpolation for *MIN6* should coincide with the *T6-U3* interpolation given in Section 3.2 if the bubble degree of freedom were constrained to:

$$\begin{aligned} w_b = &\frac{1}{3}[(b_3 - b_2)\theta_{x1} + (a_3 - a_2)\theta_{y1} + (b_1 - b_3)\theta_{x2} + (a_1 - a_3)\theta_{y2} + (b_2 - b_1)\theta_{x3} \\ &+ (a_2 - a_1)\theta_{y3}] + \frac{2}{3}[(b_2 - b_1)\theta_{x4} + (a_2 - a_1)\theta_{y4} + (b_3 - b_2)\theta_{x5} + (a_3 - a_2)\theta_{y5} \\ &+ (b_1 - b_3)\theta_{x6} + (a_1 - a_3)\theta_{y6}]. \end{aligned} \tag{25}$$

It should be made clear that the shear strain distribution of a certain order along an arbitrary direction is the basic underlying condition from which the *MINn* family of elements has been derived, while the shear strain distribution of a certain order along a direction parallel to the element sides is a consequence, rather than the origin of the family of elements presented in Section 3. The presented methodology generates the linked interpolation from the underlying interpolation functions developed for the beam elements and may be consistently and straight-forwardly applied to triangular plate elements of arbitrary order. In contrast, the *MINn* methodology requires a symbolic manipulation of algebraic expressions which get progressively more complicated as the order of the element is raised.

5. Finite element stiffness matrix and load vector

The earlier interpolations may be written in matrix form as:

$$w = \mathbf{I}_{ww}\mathbf{w} + \mathbf{N}_{w\theta}\boldsymbol{\theta}_{x,y} + \mathbf{N}_{wb}\mathbf{w}_b, \tag{26}$$

$$\begin{Bmatrix} \theta_x \\ \theta_y \end{Bmatrix} = \mathbf{I}_{\theta\theta}\boldsymbol{\theta}_{x,y}, \tag{27}$$

where $\mathbf{I}_{ww}$ is a matrix of all interpolation functions concerning the nodal displacement parameters with the dimension $1 \times N_{nd}$, where $N_{nd} = n(n+1)/2$ and n is the number of nodes per element side. Also, $\mathbf{w}$ is the vector of nodal displacement parameters with the dimension N_{nd}: $\mathbf{w}^T = \langle w_1 \ldots w_n \rangle$, $\mathbf{N}_{w\theta}$ is the matrix of all linked interpolation functions with the dimension $1 \times 2N_{nd}$ and $\boldsymbol{\theta}_{x,y}$ is the vector of nodal rotations in global coordinate directions with the dimension $2N_{nd}$: $\boldsymbol{\theta}_{x,y}^T = \langle \theta_{x1}, \theta_{y1} \ldots \theta_{xn}, \theta_{yn} \rangle$. Further, $\mathbf{N}_{wb}$ is the matrix of bubble interpolation functions given in equation (13) or equation (17) with the dimension $1 \times N_b$ and $\mathbf{w}_b$ is the bubble parameter vector with the dimension $N_b = n - 2$: $\mathbf{w}_b^T = \langle w_{b,1} \ldots w_{b,n-2} \rangle$, only for $n \geq 2$. $\mathbf{I}_{\theta\theta}$ is again the matrix of all interpolation functions concerning rotational parameters described in equations (8), (9), (11) and (12) or equations (15) and (16) and has the dimension $2 \times 2N_{nd}$.

The formation of the element stiffness matrix and the external load vector for the interpolation functions defined in this way follows the standard finite-element procedure described in text-books (Bathe, 1989; Hughes, 2000; Zienkiewicz *et al.*, 2005). A functional of the total energy of the system is given in equation (6) and from the stationarity condition for the total potential energy of an element, a system of algebraic equations is derived:

$$\begin{bmatrix} \mathbf{K}_{\mathbf{S}ww} & \mathbf{K}_{\mathbf{S}w\theta}^T & \mathbf{K}_{\mathbf{S}wb}^T \\ \mathbf{K}_{\mathbf{S}w\theta} & \mathbf{K}_{\mathbf{B}\theta\theta} + \mathbf{K}_{\mathbf{S}\theta\theta} & \mathbf{K}_{\mathbf{S}b\theta}^T \\ \mathbf{K}_{\mathbf{S}wb} & \mathbf{K}_{\mathbf{S}b\theta} & \mathbf{K}_{\mathbf{S}bb} \end{bmatrix} \begin{bmatrix} \mathbf{w} \\ \boldsymbol{\theta}_{x,y} \\ \mathbf{w}_b \end{bmatrix} = \begin{bmatrix} \mathbf{f}_w \\ \mathbf{f}_\theta \\ \mathbf{f}_b \end{bmatrix},$$

where vectors $\mathbf{f}_w$, $\mathbf{f}_\theta$ and $\mathbf{f}_b$ are the terms due to external loading. The submatrices in the stiffness matrix follow:

$$\begin{aligned}
\mathbf{K}_{\mathbf{B}\theta\theta} &= \int_A (\mathbf{L}\mathbf{I}_{\theta\theta})^T \mathbf{D_b} (\mathbf{L}\mathbf{I}_{\theta\theta}) dA \\
\mathbf{K}_{\mathbf{S}ww} &= \int_A (\nabla \mathbf{I}_{ww})^T \mathbf{D_s} (\nabla \mathbf{I}_{ww}) dA \\
\mathbf{K}_{\mathbf{S}bb} &= \int_A (\nabla \mathbf{N}_{wb})^T \mathbf{D_s} (\nabla \mathbf{N}_{wb}) dA \\
\mathbf{K}_{\mathbf{S}\theta\theta} &= \int_A (\mathbf{e}\mathbf{I}_{\theta\theta} + \nabla \mathbf{N}_{w\theta})^T \mathbf{D_s} (\mathbf{e}\mathbf{I}_{\theta\theta} + \nabla \mathbf{N}_{w\theta}) dA \\
\mathbf{K}_{\mathbf{S}w\theta} &= \int_A (\mathbf{e}\mathbf{I}_{\theta\theta} + \nabla \mathbf{N}_{w\theta})^T \mathbf{D_s} (\nabla \mathbf{I}_{ww}) dA \\
\mathbf{K}_{\mathbf{S}wb} &= \int_A (\nabla N_{wb})^T \mathbf{D_s} (\nabla \mathbf{I}_{ww}) dA \\
\mathbf{K}_{\mathbf{S}b\theta} &= \int_A (\nabla N_{wb})^T \mathbf{D_s} (\mathbf{e}\mathbf{I}_{\theta\theta} + \nabla \mathbf{N}_{w\theta}) dA
\end{aligned}$$

where $\mathbf{L}$ and ∇ are the differential operators from equations (2) and (3) acting on the interpolation functions in equations (27) and (26), respectively, while $\mathbf{e}$ is a transformation matrix given in equation (2).

6. Test examples

In all the examples the results for the elements *T3-U2*, *T6-U3* and *T10-U4* are compared to the mixed-type element of Auricchio and Taylor (1995) denoted as *T3-LIM* and integrated in FEAP (a finite element analysis program) by the same authors, or to the *T3BL* element (Taylor and Auricchio, 1993). Also, comparison is made to the *MIN6* element (Liu and Riggs, 2005) and the hybrid-type element 9βQ4 (de Miranda and Ubertini, 2006) as well as the linked-interpolation quadrilateral elements *Q4-U2*, *Q9-U3* and *Q16-U4* (Ribarić and Jelenić, 2012).

6.1 Patch test and eigenanalysis of the stiffness matrix

Consistency of the developed elements is tested for the constant strain conditions on the patch example with ten elements, covering a rectangular domain of a plate as shown in Figure 10. The displacements and rotations for the four internal nodes within the patch are checked for the specific displacements and rotations given at the four external nodes (Chen and Cheung, 2000, 2001; Chen, 2006; Chen *et al.*, 2009). The plate properties are $E = 10^5$, $\nu = 0.25$, $k = 5/6$, while two different thicknesses corresponding to a thick and a thin plate extremes are considered: $h = 1.0$ and $h = 0.01$.

Two strain-stress states are analysed (Chen *et al.*, 2009):

(1) *Constant bending state*

Displacements and rotations are expressed, respectively, by:

$$w = (1 + x + 2y + x^2 + xy + y^2)/2, \quad \theta_x = (2 + x + 2y)/2, \quad \theta_y = -(1 + 2x + y)/2.$$

The exact displacements and rotations at the internal nodes and the exact strains and stress resultants at every integration point are expected. The moments are constant $M_x = M_y = -11{,}111.11\,h^3$, $M_{xy} = -33{,}333.33\,h^3$ and the shear forces vanish ($S_x = S_y = 0$).

(2) *Constant shear state*

Displacements and rotations are expressed, respectively, by:

$$w = -\frac{h^2}{5(1-\nu)}(14x + 18y) + x^3 + 2y^3 + 3x^2y + 4xy^2, \quad \theta_x = 3x^2 + 8xy + 6y^2,$$
$$\theta_y = -(3x^2 + 6xy + 4y^2).$$

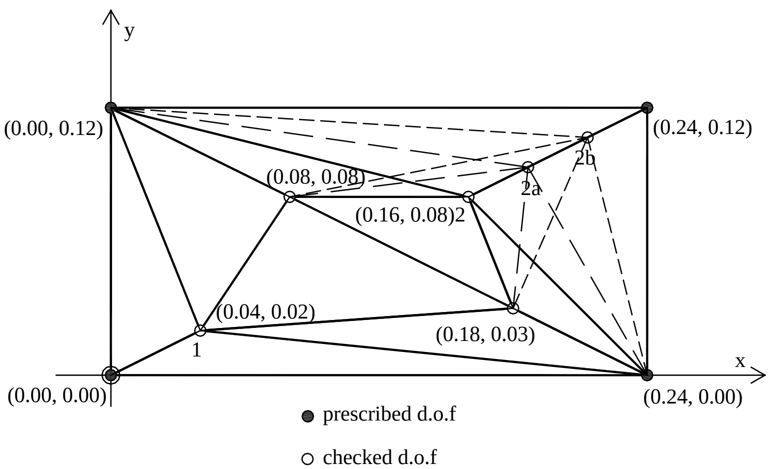

Figure 10.
Element patch for consistency assessment of three-node elements

The exact displacements and rotations at the internal nodes and the exact strains and stress resultants at every integration point are expected again. The shear forces are constant $S_x = -124{,}400.0\,h^3$ and $S_y = -160{,}000.0\,h^3$ in every Gauss point and the moments are linearly distributed according to:

$$M_x = -\frac{Eh^3}{12(1-\nu^2)}[x(6+8\nu)+y(6+12\nu)],$$
$$M_y = -\frac{Eh^3}{12(1-\nu^2)}[x(8+6\nu)+y(12+6\nu)] \text{ and}$$
$$M_{xy} = -\frac{Eh^3}{12(1-\nu^2)}\frac{1-\nu}{2}(12x+16y).$$

The three-node triangle element *T3-U2* is tested on the patch given in Figure 10. For the given values for the displacements and rotations at the external nodes calculated from the above data, the displacements and rotations at the internal nodes as well as the bending and torsional moments and the shear forces at the integration points are calculated and found out to correspond exactly to the analytical results given above for the constant bending test, but not for the constant shear test. It should be noted that the constant shear test performed here is related to a linear change in curvature (third-order cylindrical bending) and in fact by definition requires an element to enable cubic distribution of the displacement field and the quadratic distribution of the rotation fields, for which the analysed element is not designed. This test should not be mistaken for the constant shear test with no curvature as a consequence of a suitable choice of distributed moment loadings (de Miranda and Ubertini, 2006), which the analysed element also passes.

The six-node triangle element *T6-U3* is tested on the similar patch example (the mesh is given in Figure 11). Again, only the displacements and rotations at the boundary nodes are given (eight displacements and 16 rotations), while all the internal nodal displacements and rotations are to be calculated by the finite-element

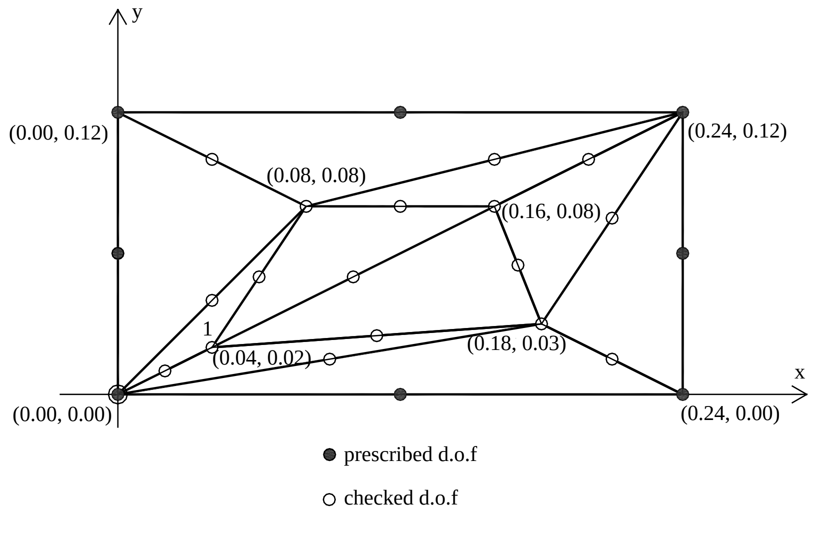

Figure 11. Element patch for consistency assessment of six-node elements

solution procedure. In fact, they are calculated exactly for both the constant bending and the constant shear test. The moments and shear forces at the integration points are also exact.

The same patch tests are also successfully performed by the ten-node elements *T10-U4*, where 48 parameters for the degrees of freedom are prescribed and 108 others are checked (Figure 12).

The results of the patch tests for all three proposed elements are given in Table I for the displacement at node 1 with co-ordinates (0.04, 0.02). The results are not altered if any of the internal nodes changes its position in the mesh (for example node 2 in Figure 10) for *T3-U2* element's constant curvature test or for *T6-U3* and *T10-U4* elements in both tests. The results of the patch tests are not sensitive to mesh distortion.

Furthermore, the quartic interpolation for the displacement field would enable the ten-node element *T10-U4* to exactly reproduce even the cylindrical bending of the fourth order.

For stability assessment of the elements, a patch test must be obviously satisfied, but the eigenanalysis on the single element should be also checked out (Auricchio and

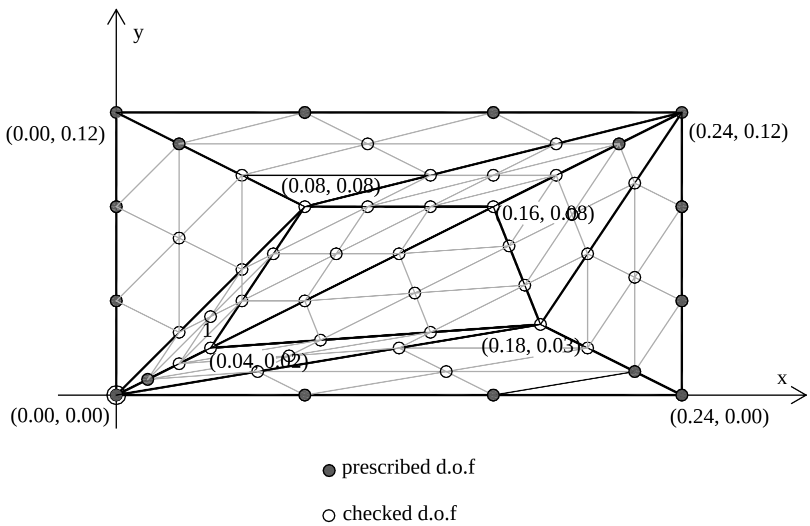

Figure 12.
Element patch for consistency assessment of ten-node elements

Table I.
The patch test results for the proposed elements

Elements	Patch test for constant curvature $h = 1.0$	$h = 0.01$	Result	Patch test for constant shear $h = 1.0$	$h = 0.01$	Result
T3-U2(*2*)	0.5414000	0.5414000	Pass	− 0.2455871	0.000318188	Fail
T3-U2(*2a*)	0.5414000	0.5414000	Pass	− 0.2455964	0.000320889	Fail
T3-U2(*2b*)	0.5414000	0.5414000	Pass	− 0.2456247	0.000326492	Fail
T6-U3	0.5414000	0.5414000	Pass	− 0.2450933	0.000215467	Pass
T10-U4	0.5414000	0.5414000	Pass	− 0.2450933	0.000215467	Pass
Analytical solution	0.5414	0.5414		− 0.245093333	0.000215467	

Note: Displacement at point 1: w_1

Taylor, 1994, 1995). Several cases of span-to-thickness ratio are considered: $L/h = 10$, $L/h = 1{,}000$ and $L/h = 100{,}000$ (Figure 13). In eigenanalysis the bending stiffness is kept constant by scaling the Young modulus proportionally to $(1/h)^3$. The elements have always the correct number of zero eigenvalues that correspond to rigid body modes. The *T3-U2* element has three eigenvalues that are associated with shear, which experience considerable growth as the element thickness is reduced indicating a propensity of the element to lock. The other three eigenvalues are bending dependent and they remain constant. The results are given in Table II. In *T6-U3* and *T10-U4* elements there also exist the growing shear-related eigenvalues, but there is also an increased number of the eigenvalues which remain constant (Tables III and IV). It will be shown in Sections 6.2-6.5 that, in spite of the growing eigenvalues, these elements considerably reduce or completely eliminate the locking effect.

6.2 Clamped square plate

In this example, a square plate with clamped edges is considered. Only one quarter of the plate is modeled with symmetric boundary conditions imposed on the symmetry lines. Two ratios of span versus thickness are analysed, $L/h = 10$ representing a relatively thick plate and $L/h = 1{,}000$ representing its thin counterpart. The loading on the plate is uniformly distributed of magnitude $q = 1$. The plate material properties are $E = 10.92$ and $\nu = 0.3$.

The numerical results for the mesh pattern in Figure 14 are given in Tables V and VII and compared to the elements presented in Taylor and Auricchio (1993) and Auricchio and Taylor (1995) based on the mixed approach. The dimensionless results $w^* = w/(qL^4/100D)$ and $M^* = M/(qL^2/100)$, where $D = Eh^3/(12(1 - v^2))$ and L is the plate span, given in these tables are related to the central displacement of the plate and the bending moment at the integration point nearest to the centre of the plate. The number of elements per mesh in these tables is given for one quarter of the structure as shown in Figure 14 for the 4×4 mesh consisting of 32 elements.

Clearly, all the new elements converge towards the same solution as the elements from the literature, and the higher-order elements exhibit an expected faster convergence rate. Still, the lowest-order element *T3-U2* is somewhat inferior to *T3BL*, which is not surprising knowing that that element is actually based on the linked interpolation as in *T3-U2* on top of which additional improvements are made.

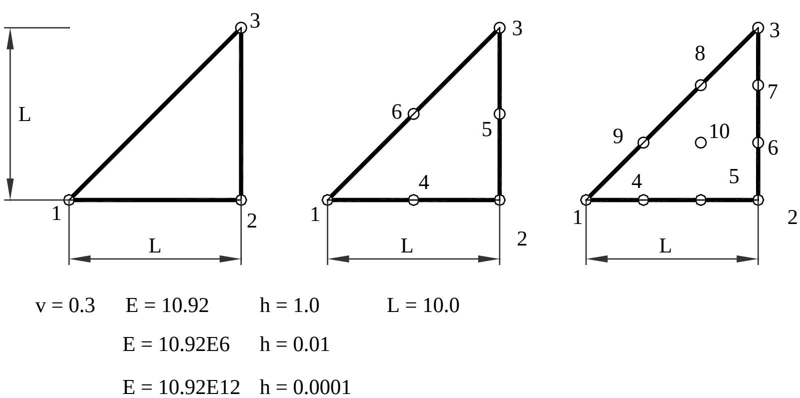

Figure 13. Single element eigenanalysis is performed over the right angle triangle geometry

Table II.
Right angle triangle element *T3-U2*. Eigenvalues of the element stiffness matrix

L/h	1	2	3	4	5	6	7	8	9
10	$9.2916 \times 10^{+01}$	$7.0841 \times 10^{+01}$	$1.8644 \times 10^{+01}$	$1.5284 \times 10^{+00}$	4.6439×10^{-01}	3.0558×10^{-01}	-8.0124×10^{-15}	-1.5722×10^{-15}	9.1870×10^{-16}
1,000	$9.2750 \times 10^{+05}$	$7.0727 \times 10^{+05}$	$1.8523 \times 10^{+05}$	$1.5289 \times 10^{+00}$	4.6818×10^{-01}	3.0603×10^{-01}	-2.1391×10^{-11}	1.5980×10^{-11}	-7.3091×10^{-12}
100,000	$9.2750 \times 10^{+09}$	$7.0727 \times 10^{+09}$	$1.8523 \times 10^{+09}$	$1.5289 \times 10^{+00}$	4.6818×10^{-01}	3.0603×10^{-01}	-3.6371×10^{-07}	2.8079×10^{-07}	-1.3488×10^{-07}

Table III. Right angle triangle element *T6-U3*. Eigenvalues of the element stiffness matrix

L/h	1 10	2 11	3 12	4 13	5 14	6 15	7 16	8 17	9 18
10	$7.2241 \times 10^{+01}$	$6.9624 \times 10^{+01}$	$3.4600 \times 10^{+01}$	$1.8202 \times 10^{+01}$	$1.7593 \times 10^{+01}$	$9.8251 \times 10^{+00}$	$8.5411 \times 10^{+00}$	$7.4942 \times 10^{+00}$	$4.1303 \times 10^{+00}$
	$1.4523 \times 10^{+00}$	$1.2201 \times 10^{+00}$	4.1086×10^{-01}	2.0232×10^{-01}	1.1930×10^{-01}	5.8308×10^{-02}	9.5929×10^{-16}	-7.9061×10^{-16}	1.5370×10^{-17}
1,000	$7.1634 \times 10^{+05}$	$6.9196 \times 10^{+05}$	$3.3617 \times 10^{+05}$	$1.7437 \times 10^{+05}$	$1.6940 \times 10^{+05}$	$9.0657 \times 10^{+04}$	$7.9059 \times 10^{+04}$	$6.4199 \times 10^{+04}$	$4.2286 \times 10^{+00}$
	$1.5912 \times 10^{+00}$	$1.3117 \times 10^{+00}$	4.2637×10^{-01}	2.1623×10^{-01}	1.2203×10^{-01}	5.9724×10^{-02}	-3.7196×10^{-11}	-2.1338×10^{-11}	6.3023×10^{-12}
100,000	$7.1633 \times 10^{+09}$	$6.9196 \times 10^{+09}$	$3.3617 \times 10^{+09}$	$1.7437 \times 10^{+09}$	$1.6940 \times 10^{+09}$	$9.0656 \times 10^{+08}$	$7.9058 \times 10^{+08}$	$6.4198 \times 10^{+08}$	$4.2286 \times 10^{+00}$
	$1.5913 \times 10^{+00}$	$1.3117 \times 10^{+00}$	4.2637×10^{-01}	2.1623×10^{-01}	1.2203×10^{-01}	5.9724×10^{-02}	3.5318×10^{-07}	1.3047×10^{-07}	2.6057×10^{-08}

Table IV.
Right angle triangle element *T6-U3*.
Eigenvalues of the element stiffness matrix

	1	2	3	4	5	6	7	8	9
	10	11	12	13	14	15	16	17	18
	19	20	21	22	23	24	25	26	27
L/h	28	29	30						
10	$6.3908 \times 10^{+01}$	$5.5783 \times 10^{+01}$	$5.4853 \times 10^{+01}$	$4.6366 \times 10^{+01}$	$4.5212 \times 10^{+01}$	$3.8827 \times 10^{+01}$	$1.4491 \times 10^{+01}$	$1.3399 \times 10^{+01}$	$1.1589 \times 10^{+01}$
	$9.5035 \times 10^{+00}$	$7.8069 \times 10^{+00}$	$7.7479 \times 10^{+00}$	$6.8130 \times 10^{+00}$	$5.7991 \times 10^{+00}$	$4.8800 \times 10^{+00}$	$4.0689 \times 10^{+00}$	$3.5945 \times 10^{+00}$	$2.1769 \times 10^{+00}$
	$1.4725 \times 10^{+00}$	$1.1786 \times 10^{+00}$	5.0913×10^{-01}	3.7071×10^{-01}	3.4339×10^{-01}	2.1503×10^{-01}	1.5811×10^{-01}	8.4796×10^{-02}	4.4989×10^{-02}
	-3.5718×10^{-15}	3.4046×10^{-15}	-2.4693×10^{-15}						
1,000	$6.1038 \times 10^{+05}$	$5.2861 \times 10^{+05}$	$5.1867 \times 10^{+05}$	$4.5341 \times 10^{+05}$	$4.4273 \times 10^{+05}$	$3.7483 \times 10^{+05}$	$1.3059 \times 10^{+05}$	$1.2731 \times 10^{+05}$	$9.6433 \times 10^{+04}$
	$7.7227 \times 10^{+04}$	$7.2023 \times 10^{+04}$	$5.4640 \times 10^{+04}$	$5.2870 \times 10^{+04}$	$3.6074 \times 10^{+04}$	$3.0501 \times 10^{+04}$	$6.4742 \times 10^{+00}$	$4.4053 \times 10^{+00}$	$2.3983 \times 10^{+00}$
	$1.7292 \times 10^{+00}$	$1.5469 \times 10^{+00}$	5.4943×10^{-01}	4.1616×10^{-01}	3.8820×10^{-01}	2.3809×10^{-01}	1.6841×10^{-01}	8.8825×10^{-02}	4.6435×10^{-02}
	1.6798×10^{-11}	-1.5475×10^{-11}	1.0763×10^{-13}						
100,000	$6.1038 \times 10^{+09}$	$5.2861 \times 10^{+09}$	$5.1867 \times 10^{+09}$	$4.5341 \times 10^{+09}$	$4.4273 \times 10^{+09}$	$3.7483 \times 10^{+09}$	$1.3059 \times 10^{+09}$	$1.2731 \times 10^{+09}$	$9.6432 \times 10^{+08}$
	$7.7225 \times 10^{+08}$	$7.2022 \times 10^{+08}$	$5.4639 \times 10^{+08}$	$5.2868 \times 10^{+08}$	$3.6073 \times 10^{+08}$	$3.0500 \times 10^{+08}$	$6.4742 \times 10^{+00}$	$4.4054 \times 10^{+00}$	$2.3984 \times 10^{+00}$
	$1.7293 \times 10^{+00}$	$1.5469 \times 10^{+00}$	5.4944×10^{-01}	4.1616×10^{-01}	3.8821×10^{-01}	2.3809×10^{-01}	1.6841×10^{-01}	8.8826×10^{-02}	4.6435×10^{-02}
	-5.3269×10^{-07}	8.9363×10^{-08}	-1.1525×10^{-08}						

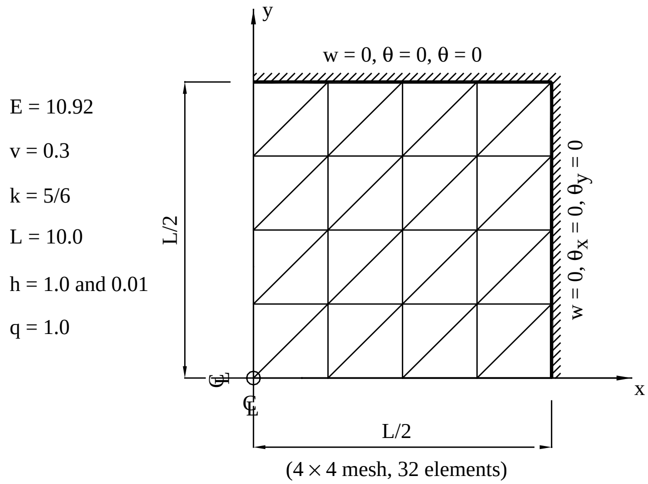

Figure 14.
A quarter of the square plate with clamped boundary conditions under uniform load (32-element mesh)

Table V.
Clamped square plate

	T3-U2		*T6-U3*		*T10-U4*	
Element mesh	w^*	M^*	w^*	M^*	w^*	M^*
1 × 1	0.023810	–	0.133334	3.31099	0.150650	2.29043
2 × 2	0.107572	1.67455	0.150247	2.63888	0.150386	2.31564
4 × 4	0.141724	2.20593	0.150447	2.39797	0.150455	2.31955
8 × 8	0.148406	2.29114	0.150458	2.33941	0.1504622	2.31996
16 × 16	0.149959	2.31216	0.1504621	2.32486	0.1504626	2.31998
32 × 32	0.150339	2.31796	0.1504625	2.32121		
64 × 64	0.150432	2.31948				
Ref. sol. (Naumenko *et al.*, 2001)	0.150191		0.150191		0.150191	
	T3BL (Taylor and Auricchio, 1993)		*MIN6*			
Element mesh	w^*	M^*	w^*	M^*		
1 × 1			0.128411	3.21000		
2 × 2	0.126275	1.59649	0.150072	2.63367		
4 × 4	0.144973	2.15009	0.150435	2.39768		
8 × 8	0.149114	2.27741	0.150457	2.33937		
16 × 16	0.150131	2.30930	0.1504620	2.32486		
32 × 32	0.150382	2.31734	0.1504625	2.32121		
64 × 64	0.150443	2.31933				
Ref. sol. (Naumenko *et al.*, 2001)	0.150191		0.150191			

Note: Displacement and moment at the centre, $L/h = 10$

The minute differences between the results of *T6-U3* and *MIN6* are attributed to the slight difference in these elements as explained in Section 4.2.

Comparing the present triangular linked-interpolation elements to their quadrilateral counterparts (Ribarić and Jelenić, 2012) shows that for the same number of the degrees of freedom the latter, converge a little faster (Table VI).

Convergence of the central displacement for the thick-plate case is presented in Figure 15, with respect to the number of degrees of freedom (in logarithmic scale).

Element mesh	*9βQ4* (de Miranda and Ubertini, 2006) w^*	M^*	*Q4-U2* w^*	M^*	*Q9-U3* w^*	M^*	*Q16-U4* w^*	M^*
1 × 1			0.02679	0.0	0.15059	3.40254	0.14974	2.08359
2 × 2	0.1625190	2.83817	0.11920	2.02221	0.15046	2.45416	0.15041	2.30177
4 × 4	0.1534432	2.44825	0.14361	2.25778	0.15044	2.34636	0.1504579	2.31802
8 × 8	0.1511805	2.35119	0.14876	2.30471	0.15046	2.32618	0.1504624	2.31966
16 × 16	0.1506379	2.32770	0.15004	2.31616	0.1504622	2.32152	0.1504626	2.31991
32 × 32	0.1505061	2.32191	0.15036	2.31903	0.1504625	2.32037		
64 × 64			0.15044	2.31975				
Ref. sol. (Naumenko *et al.*, 2001)	0.150191		0.150191		0.150191		0.150191	

Table VI.
Clamped square plate

Note: Displacement and moment at the centre using a quadrilateral hybrid element (de Miranda and Ubertini, 2006) and linked-interpolation elements (Ribarić and Jelenić, 2012), $L/h = 10$

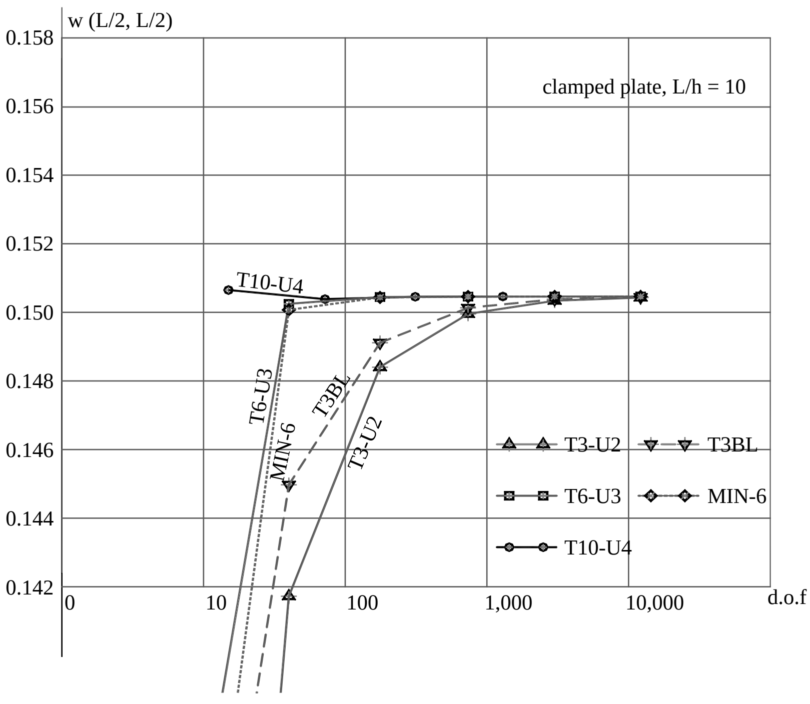

Figure 15.
Convergence of the transverse displacement at the centre for $L/h = 10$

Best convergence with respect to the number of degrees of freedom can be observed in elements with higher-order linked interpolation and it may be concluded that for the thick clamped plate the present elements converge competitively for a comparable number of degrees of freedom.

The M_x moment distribution along the x-axis is computed at the Gauss points closest to the axis and, beginning from the centre point of the plate, shown in Figure 16. These results are the same as the results for the moment M_y along the y-direction. For *T3-U2* element, the moment is constant across the element, owing to its dependence on the derivatives of rotations (8) and (9) in both directions. For elements *T6-U3* and *T10-U4*, the moment distribution is accordingly linear or quadratic, respectively, and the results converge towards the exact distribution fast. Similar observations may be made for the distribution of the shear-stress resultants.

For the thin plate case shown in Table VII, the elements *T3-U2* and *T6-U3* suffer from some shear locking when the meshes are coarse, but as expected they converge to the correct result. The higher-order elements exhibit an expected faster convergence rate.

As for the case of the thick plate, the lowest-order element *T3-U2* is still somewhat inferior to *T3BL*, while *T6-U3* is marginally better than *MIN6*. Likewise, comparing the triangular linked-interpolation elements to their quadrilateral counterparts (Ribarić and Jelenić, 2012) shows that for the same number of the degrees of freedom the latter, converge a little faster (Table VIII).

If the same example were run with a different orientation of the triangular elements (with the longest element side orthogonal to the diagonal passing through the centre of the plate) the results would turn out to be slightly worse even though for the higher-order elements the trend gets reversed as the mesh is refined. This is shown in Table IX for the thin plate case.

The differences in the results given for the two orientations (Tables VII and IX) drop below 3.3 per cent for the *T3-U2* displacement with a 16x16 mesh already.

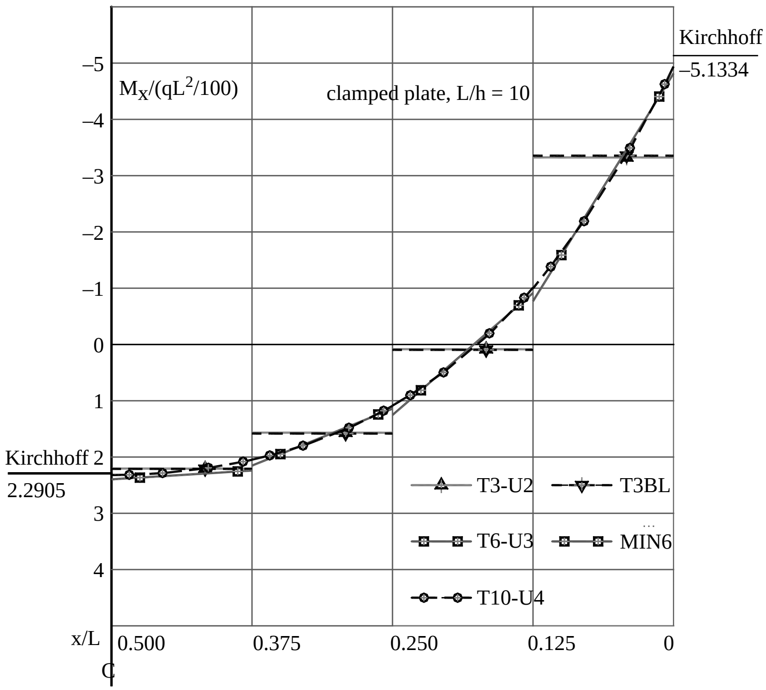

Figure 16.
Moment M_x distribution along element's Gauss points closest to the x axis on the 4×4 regular mesh for the clamped plate with $L/h = 10$

Element mesh	T3-U2 w^*	T3-U2 M^*	T6-U3 w^*	T6-U3 M^*	T10-U4 w^*	T10-U4 M^*
1 × 1			0.000069	0.00206	0.130198	4.05972
2 × 2	0.000062	0.00127	0.097869	2.03760	0.126738	2.74752
4 × 4	0.001793	0.03807	0.121256	2.44562	0.126527	2.34533
8 × 8	0.028267	0.55913	0.125905	2.38599	0.1265340	2.29246
16 × 16	0.104428	2.12079	0.1265121	2.31332	0.1265344	2.29055
32 × 32	0.124820	2.32200	0.1265341	2.29420		
64 × 64	0.126403	2.29435				
Ref. sol. (Zienkiewicz *et al.*, 1993)	0.126532	2.29051	0.126532	2.29051	0.126532	2.29051
	T3BL (Taylor and Auricchio, 1993)		*MIN6*			
Element mesh	w^*	M^*	w^*	M^*		
1 × 1			0.000061	0.00182		
2 × 2	0.093098	1.40767	0.097850	2.03613		
4 × 4	0.118006	2.10245	0.121205	2.43983		
8 × 8	0.124616	2.24825	0.125878	2.38437		
16 × 16	0.126092	2.28031	0.1265107	2.31409		
32 × 32	0.126429	2.28798	0.1265341	2.29440		
64 × 64	0.126509	2.28987				
Ref. sol. (Zienkiewicz *et al.*, 1993)	0.126532	2.29051	0.126532	2.29051		

Note: Displacement and moment at the centre, $L/h = 1{,}000$

Table VII.
Clamped square plate

6.3 Simply supported square plate

In this example the square plate as before is considered, but this time with the simply supported edges of the type SS2 (displacements and rotations around the normal to the edge set to zero) as shown in Figure 17. The same elements as before are tested and the results are given in Tables X and XII for the thick and the thin plate, respectively, compared again to the elements presented in Taylor and Auricchio (1993) and Auricchio and Taylor (1995) (Tables X-XIII).

The dimensionless results $w^* = w/(qL^4/100D)$ and $M^* = M/(qL^2/100)$ given in these tables are related to the central displacement of the plate and the bending moment at the integration point nearest to the centre of the plate. The number of elements per mesh in these tables relates to one quarter of the plate.

For the thick plate case, it can be concluded that elements *T6-U3* and *T10-U4* converge considerably faster than elements based on the mixed approach and no locking can be observed on coarse meshes, even for the three-node element *T3-U2*. In the thin plate example, locking on the coarse meshes can be observed for *T3-U2*, but higher-order elements, again, show very good convergence rate.

In contrast to the clamped plate problem, the mesh pattern used here has slightly better convergence than the mesh pattern used in that example.

6.4 Simply supported skew plate

In this example the rhombic plate is considered with the simply supported edges (this time, of the so-called soft type SS1 (Babuška and Scapolla, 1989) to test performance of the rhombic elements. The problem geometry and material properties are given in Figure 18, where an example of a 8 × 8-mesh is shown (128 triangular elements).

The same three elements as before are tested and the results are given in Tables XIV and XVIII for the thick and the thin plate, respectively. The dimensionless results

Table VIII.
Clamped square plate

Element mesh	*9βQ4* (de Miranda and Ubertini, 2006) w^*	M^*	*Q4-U2* w^*	M^*	*Q9-U3* w^*	M^*	*Q16-U4* w^*	M^*
1 × 1			0.0000027		0.00027	0.00746	0.13241	3.70328
2 × 2	0.13766768	2.745544	0.00013	− 0.0001	0.09918	2.03484	0.12646	2.40533
4 × 4	0.12938531	2.423885	0.00469	0.10731	0.12112	2.24000	0.1265288	2.29613
8 × 8	0.12725036	2.323949	0.05988	1.18496	0.12621	2.29083	0.1265343	2.29039
16 × 16	0.12671406	2.298876	0.11899	2.17415	0.1265273	2.29179	0.1265345	2.29044
32 × 32	0.12657946	2.292605	0.12600	2.28275	0.1265343	2.29086		
64 × 64			0.12648	2.28988				
Ref. sol. (Zienkiewicz *et al.*, 1993)	0.126532	2.29051	0.126532	2.29051	0.126532	2.29051	0.126532	2.29051

Note: Displacement and moment at the centre using a quadrilateral hybrid element (de Miranda and Ubertini, 2006) and linked-interpolation elements (Ribarić and Jelenić, 2012), $L/h = 1{,}000$

Element mesh	*T3-U2* w^*	M^*	*T6-U3* w^*	M^*	*T10-U4* w^*	M^*
1 × 1	0.000001		0.000057	0.00195	0.113949	2.03147
2 × 2	0.000052	0.00112	0.080795	1.09704	0.125997	2.28567
4 × 4	0.001531	0.02764	0.116226	1.87195	0.126515	2.29025
8 × 8	0.025112	0.38406	0.125363	2.18328	0.1265340	2.29044
16 × 16	0.100985	1.64321	0.126496	2.27223	0.1265344	2.29050
32 × 32	0.124358	2.20020	0.1265336	2.28838		
64 × 64	0.126356	2.28191				
Ref. sol. (Zienkiewicz *et al.*, 1993)	0.126532	2.29051	0.126532	2.29051	0.126532	2.29051

Table IX.
Clamped square plate

Note: Displacement and moment at the centre using opposite orientation of triangular elements in the mesh, $L/h = 1{,}000$

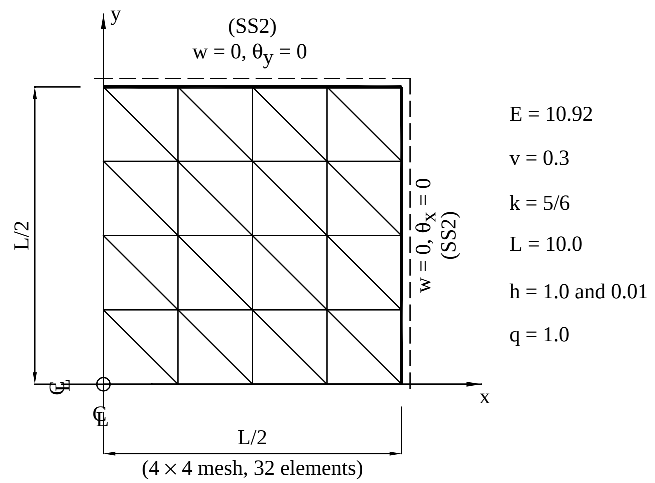

Figure 17.
A quarter of the square plate with simply supported boundary conditions (SS2), under uniform load (32-element mesh)

$w^* = w/(qL^4/10^4D), M_{11}^* = M_{11}/(qL^2/100)$ and $M_{22}^* = M_{22}/(qL^2/100)$ are related to the central displacement of the plate and the principal bending moments in diagonal directions at the integration point nearest to the centre of the plate.

The tested example has two orthogonal axes of symmetry, A-C-B and D-C-E, and only one triangular quarter may be taken for analysis (Hughes, 2000; Hughes and Tezduyar, 1981). Since there is a singularity in the moment field at the obtuse vertex, this test example is a difficult one. Even more, the analytical solution (Morley, 1962) reveals that moments in the principal directions near the obtuse vertex have opposite signs.

In contrast to the earlier examples, it must be noted that here the new displacement-based elements perform worse than the elements given in Taylor and Auricchio (1993) and Auricchio and Taylor (1995), both for the thick and the thin plate examples. Tables XIV and XVIII now reveal slightly more pronounced differences in the results obtained using elements *T6-U3* and *MIN6*, where the latter are somewhat worse, apparently owing to the absence of the internal bubble parameter present in *T6-U3* (Section 4.2). Also, from Tables XV and XIX it is apparent that for this test

Element mesh	w^*	M^*	w^*	M^*	w^*	M^*
	T3-U2		*T6-U3*		*T10-U4*	
1 × 1	0.337426	3.38542	0.392336	4.67154	0.427715	4.75435
2 × 2	0.387559	4.24192	0.425236	4.86395	0.427289	4.78646
4 × 4	0.418375	4.71153	0.427160	4.81585	0.4272843	4.78851
8 × 8	0.425129	4.78211	0.427276	4.79595	0.4272842	4.78863
16 × 16	0.426739	4.78913	0.4272837	4.79050	0.4272842	4.78862
32 × 32	0.427145	4.78913	0.4272842	4.78910		
64 × 64	0.427249	4.78883				
Navier series ref. (Zienkiewicz *et al.*, 1993)	0.427284	4.78863	0.427284	4.78863	0.427284	4.78863
	T3BL (Taylor and Auricchio, 1993)		*MIN6*		*T3-LIM* (Auricchio and Taylor, 1995)	
1 × 1			0.394395	4.63782		
2 × 2	0.403591	4.48351	0.425509	4.85815	0.40786	4.0918
4 × 4	0.421194	4.74389	0.427183	4.81531	0.42293	4.6063
8 × 8	0.425688	4.78521	0.427278	4.79591	0.42627	4.7398
16 × 16	0.426869	4.78940	0.427284	4.79049	0.42704	4.7755
32 × 32	0.427177	4.78915	0.427284	4.78910	0.42723	4.7852
64 × 64	0.427257	4.78883				
Navier series ref. (Zienkiewicz *et al.*, 1993)	0.427284	4.78863	0.427284	4.78863	0.427284	4.78863

Note: Displacement and moment at the centre, $L/h = 10$

Table X. Simply supported square plate (SS2) under uniformly distributed load

Element mesh	*9βQ4* (de Miranda and Ubertini, 2006) w^*	M^*	*Q4-U2* w^*	M^*	*Q9-U3* w^*	M^*	*Q16-U4* w^*	M^*
1 × 1			0.26102	2.88202	0.42983	5.33564	0.42717	4.66623
2 × 2	0.4286943	5.264135	0.41163	4.66892	0.42749	4.86404	0.4272820	4.77762
4 × 4	0.4276333	4.905958	0.42448	4.77207	0.42730	4.80320	0.4272842	4.78712
8 × 8	0.4273690	4.817645	0.42664	4.78515	0.42729	4.79203	0.4272842	4.78833
16 × 16	0.4273052	4.795864	0.42713	4.78781	0.42728	4.78947	0.4272842	4.78857
32 × 32	0.4272895	4.790443	0.42725	4.78843	0.42728	4.78885		
64 × 64			0.4272744	4.78859				
Navier series ref. (Zienkiewiczetal., 1993)	0.427284	4.78863	0.427284	4.78863	0.427284	4.78863	0.427284	4.78863

Note: Displacement and moment at the centre using a quadrilateral hybrid element (de Miranda and Ubertini, 2006) and linked-interpolation elements (Ribarić and Jelenić, 2012), $L/h = 10$

Table XI. Simply supported square plate (SS2) under uniformly distributed load

example the new triangular family of linked-interpolation elements is in fact superior to the family of quadrilateral linked-interpolation elements presented in Ribarić and Jelenić (2012).

The mesh pattern chosen for computing the results in Table XIV is the best among the uniformly distributed meshes. For example, meshes (b) and (c) in Figure 19 give less good results for the similar numbers of degrees of freedom as can be noticed in Tables XVI and XVII.

Table XII.
Simply supported square plate (SS2) under uniformly distributed load

Element mesh	w^*	M^*	w^*	M^*	w^*	M^*
	T3-U2		*T6-U3*		*T10-U4*	
1×1	0.325522	3.38542	0.325543	2.51970	0.405992	4.53393
2×2	0.325541	3.07155	0.389672	3.56892	0.406198	4.78210
4×4	0.326331	2.67663	0.402526	4.25254	0.406234	4.78844
8×8	0.339027	2.80820	0.405659	4.62852	0.4062373	4.78860
16×16	0.383803	4.01006	0.406211	4.76246	0.4062374	4.78861
32×32	0.403889	4.67235	0.406237	4.78543		
64×64	0.406062	4.77806				
Navier series ref. (Zienkiewicz *et al.*, 1993)	0.406237	4.78863	0.406237	4.78863	0.406237	4.78863
	T3BL (Taylor and Auricchio, 1993)		*MIN6*		*T3-LIM* (Auricchio and Taylor, 1995)	
1×1			0.325542	2.51962		
2×2	0.377793	4.26461	0.389669	3.56861	0.38412	4.0831
4×4	0.399068	4.65804	0.402518	4.25114	0.40114	4.6071
8×8	0.404642	4.76074	0.405646	4.62584	0.40503	4.7408
16×16	0.405871	4.78282	0.406209	4.76157	0.40594	4.7759
32×32	0.406150	4.78747	0.406237	4.78525	0.40616	4.7853
64×64	0.406216	4.78844				
Navier series ref. (Zienkiewicz *et al.*, 1993)	0.406237	4.78863	0.406237	4.78863	0.406237	4.78863

Note: Displacement and moment at the centre, $L/h = 1{,}000$

Table XIII.
Simply supported square plate (SS2) under uniformly distributed load

Element mesh	*9βQ4* (de Miranda and Ubertini, 2006) w^*	M^*	*Q4-U2* w^*	M^*	*Q9-U3* w^*	M^*	*Q16-U4* w^*	M^*
1×1			0.0000008	0.00093	0.35527	3.67992	0.41220	5.49186
2×2	0.4063653	5.241563	0.0031093	0.03842	0.39807	4.66131	0.40647	4.85587
4×4	0.4063062	4.904153	0.055621	0.68507	0.40475	4.76923	0.40624	4.79124
8×8	0.4062559	4.817513	0.29658	3.54861	0.40615	4.78990	0.40624	4.78843
16×16	0.4062421	4.795855	0.39706	4.68543	0.40624	4.78943	0.4062374	4.78857
32×32	0.4062386	4.790442	0.40562	4.78188	0.40624	4.78884		
64×64			0.40619	4.78764				
Navier series ref. (Zienkiewicz*etal.*, 1993)	0.406237	4.78863	0.406237	4.78863	0.406237	4.78863	0.406237	4.78863

Note: Displacement and moment at the centre using a quadrilateral hybrid element (de Miranda and Ubertini, 2006) and linked-interpolation elements (Ribarić and Jelenić, 2012), $L/h = 1{,}000$

The distribution of the principal moments between the obtuse angle at A and the centre-point C is very complex owing to the presence of singularity at A and worth particular consideration. The principal moment M_{11} acting around the in-plane normal to the shorter diagonal converges towards the exact solution satisfactorily, but for the principal moment M_{22} acting around the shorter diagonal it is obvious that this family of elements finds it difficult to follow the exact moment distribution near the

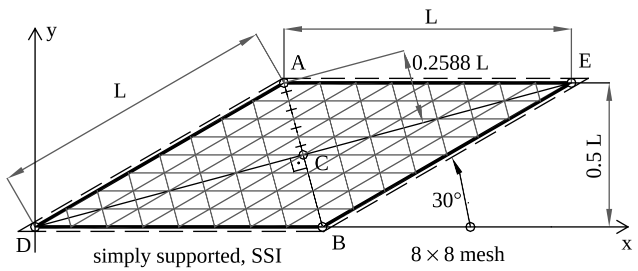

E = 10.92   L = 100

ν = 0.3   h = 1.0 and 0.10

q = 1.0

Figure 18.
A simply supported (SS1) skew plate under uniform load

		T3-U2			*T6-U3*			*T10-U4*	
Element mesh	w^*	M^*_{22}	M^*_{11}	w^*	M^*_{22}	M^*_{11}	w^*	M^*_{22}	M^*_{11}
2 × 2	0.425288	0.65647	1.35584	0.442337	1.59547	2.48908	0.259711	0.67991	1.29292
4 × 4	0.393156	1.00823	1.72050	0.391393	1.38415	2.10533	0.410136	1.17851	1.92258
8 × 8	0.376569	1.11747	1.84630	0.409028	1.18349	1.96100	0.419818	1.12774	1.94013
16 × 16	0.403524	1.09072	1.87753	0.419769	1.13814	1.95024	0.423207	1.13774	1.95080
24 × 24	0.412799	1.10360	1.92291	0.422181	1.13934	1.95222			
32 × 32	0.416390	1.11361	1.93165						
48 × 48	0.419306	1.12368	1.93948						
Ref. (Zhu, 1992)	0.423			0.423			0.423		
		T3-LIM (Auricchio and Taylor, 1995)			*MIN6*				
Element mesh	w^*	M^*_{22}	M^*_{11}	w^*	M^*_{22}	M^*_{11}			
2 × 2	0.63591	0.9207	1.7827	0.442458	1.61239	2.53454			
4 × 4	0.45819	1.0376	1.8532	0.386472	1.36333	2.10434			
8 × 8	0.43037	1.1008	1.9247	0.405862	1.16617	1.95019			
16 × 16	0.42382	1.1233	1.9376	0.418385	1.13270	1.94618			
24 × 24				0.421307	1.13604	1.94954			
32 × 32	0.42183	1.1284	1.9344						
48 × 48									
Ref. (Zhu, 1992)	0.423			0.423					

Note: Displacement and moment at the centre, $L/h = 100$

Table XIV.
Simply supported skew plate (SS1)

singularity point. These results are shown in Figure 20. It should be noted that near the singularity point the moments are getting high values of opposite signs, and there even a small relative difference between the exact result and the finite-element solution in one of the principal moments may strongly influence the other principal moment since they are related via Poisson's coefficient ($\nu = 0.3$ in this case) as shown in equation (4). Specifically, even though the finite-element solutions for the principal moment M_{11} recognise the monotonous trend of the exact solution, the fact that, as absolute values, these moments are overestimated makes it difficult for the element to provide a solution

Element mesh	9βQ4 (de Miranda and Ubertini, 2006) W^*	M_{22}^*	M_{11}^*						
2 × 2									
4 × 4	0.502900	1.354215	2.054527						
8 × 8	0.443176	1.082957	1.956494						
16 × 16	0.432211	1.149921	1.966940						
24 × 24									
32 × 32	0.426964	1.148682	1.959293						
48 × 48									
Ref. (Zhu, 1992)	0.423								
		Q4-U2			*Q9-U3*			*Q16-U4*	
Element mesh	W^*	M_{22}^*	M_{11}^*	w^*	M_{22}^*	M_{11}^*	w^*	M_{22}^*	M_{11}^*
2 × 2	0.06153	0.1349	0.3763	0.21493	0.4860	1.0536	0.28406	0.8404	1.5335
4 × 4	0.16287	0.3659	0.9226	0.32974	0.8227	1.6486	0.37778	0.9642	1.8310
8 × 8	0.29165	0.6870	1.4858	0.38719	1.0083	1.8508	0.40497	1.0681	1.8962
16 × 16	0.37449	0.9470	1.7959	0.40904	1.0890	1.9094	0.41774	1.1172	1.9345
24 × 24	0.39633	1.0348	1.8690	0.41554	1.1115	1.9279			
32 × 32	0.40536	1.0696	1.8890						
48 × 48	0.41326	1.1028	1.9213						
Ref. (Zhu, 1992)	0.423			0.423			0.423		

Note: Displacement and moment at the centre using a quadrilateral hybrid element (de Miranda and Ubertini, 2006) and linked-interpolation elements (Ribarić and Jelenić, 2012), $L/h = 100$

Table XV.
Simply supported skew plate (SS1) under uniformly distributed load

for M_{22} which would recognise the change in sign, slope and curvature evident in the exact solution. Of course, there exist techniques to reduce the error in M_{11} which, as a result, would also correct this anomaly in M_{22}, e.g. the shear correction factor concept (Figure 14 in Tessler and Hughes (1985)), an idea that has not been followed up in this paper (see Liu and Riggs (2005) for evidence and Tessler (1989)) for explanation why this concept has a diminishing effect as the interpolation order is increased) (Tables XVIII and XIX).

6.5 Simply supported circular plate

The circular plate with the simply supported edges is analysed next. The element mesh is here irregular and the influence of such irregularity is studied on the element family in consideration.

Additionally, not only the vertex nodes, but also the side nodes of the higher-order elements (six-node *T6-U3* and ten-node *T10-U4*) are now placed on the circular boundary. The edge elements are not following the straight line rule, so they must behave as curvilinear transformed triangles for which linked interpolation does not solve the patch test exactly (unless the elements become infinitesimally small). Only the transverse displacements of the nodes on the circular plate boundary are restrained and the rotations remain free (SS1 boundary condition). The results are given in Tables XX and XXI for the thick and the thin plate, respectively. The problem geometry and material properties are given in Figure 21 (only one quarter of the plate is analysed), where examples of the three-node element mesh is shown. A comparison with the linked-interpolation quadrilateral elements (Ribarić and Jelenić, 2012) is given in Table XXII:

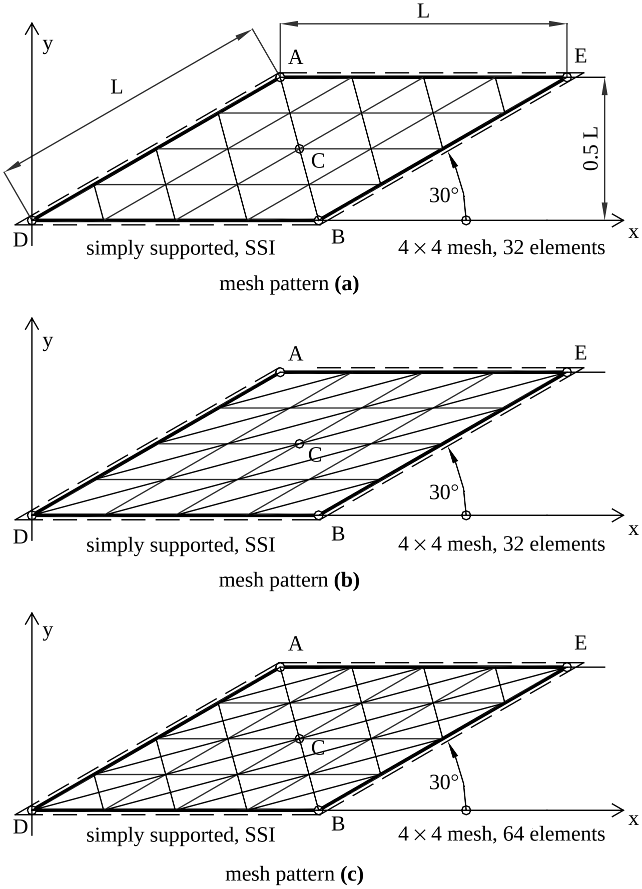

Figure 19.
A simply supported (SS1) skew plate with three different mesh patterns

Node mesh	d.o.f.	w^*	*T3-U2* M_{22}^*	M_{11}^*
2 × 2	19	0.038301	0.10796	0.33128
4 × 4	59	0.071514	0.18081	0.49677
8 × 8	211	0.170524	0.39288	0.98827
16 × 16	803	0.285767	0.67726	1.48281
24 × 24	1,779	0.337019	0.82818	1.67627
32 × 32	3,139	0.362652	0.91441	1.76454
48 × 48	7,011	0.386794	1.00372	1.84209
Ref. (Chen, 2006)		0.423		

Note: Displacement and moment at the centre, L/h = *100* – mesh pattern (b)

Table XVI.
Simply supported skew plate (SS1)

Element mesh	d.o.f.	T3-U2 w^*	T3-U2 M^*_{22}	T3-U2 M^*_{11}	T6-U3 w^*	T6-U3 M^*_{22}	T6-U3 M^*_{11}	MIN6 (Liu-Riggs) w^*	MIN6 (Liu-Riggs) M^*_{22}	MIN6 (Liu-Riggs) M^*_{11}
4 × 4	107	0.394314	0.99968	1.76770	0.442714	1.57560	2.42260	0.443030	1.58489	2.44230
8 × 8	403	0.380630	1.09990	1.85008	0.398472	1.29021	1.99636	0.394705	1.28551	1.99557
16 × 16	1,571	0.405027	1.09959	1.90959	0.412030	1.16231	1.93387	0.410138	1.15652	1.92888
Ref. (Kim and Bathe, 2009)		0.423			0.423			0.423		

Note: Displacement and moment at the centre, $L/h = 100$ − mesh pattern (c)

Table XVII. Simply supported skew plate (SS1)

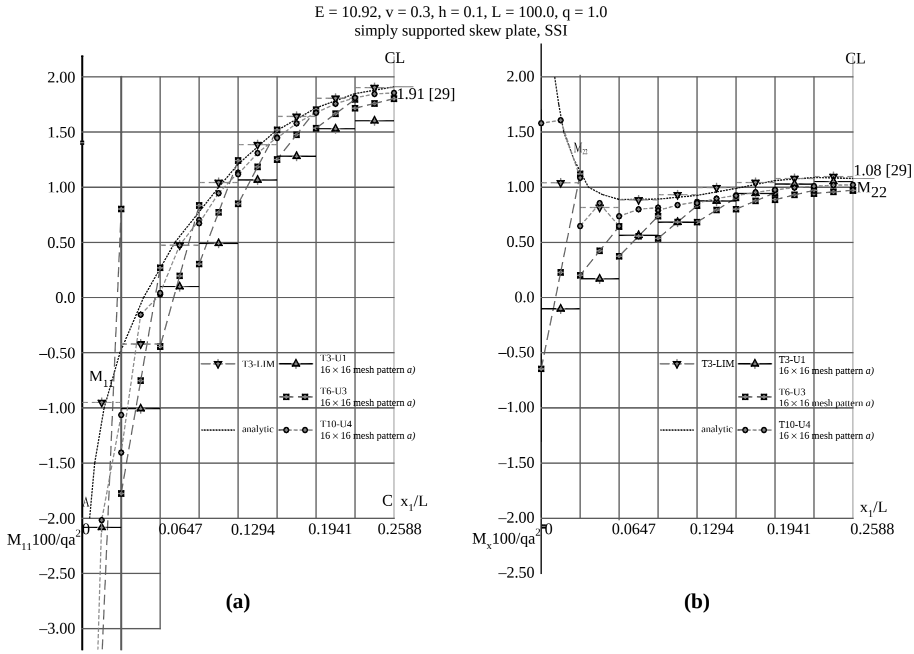

Figure 20. Simply supported skew plate under uniform load

Notes: (a) Principal moment M_{11} distribution between points A and C; (b) principal moment M_{22} distribution between points A and C

$$w_c^* = \frac{w_c}{q}\frac{100D}{(2R)^4}, \quad D = \frac{Eh^3}{12(1-\nu^2)}, \quad M_c^* = \frac{M_c}{q}\frac{100}{(2R)^2} \text{ (at closest Gauss point)}$$

$$M_x = M_y = M_c - \text{moment at the central point}$$

In Table XXIII the results for the simply supported circular plate subject to a concentrated load at the center point are given. The geometry and material properties

Element mesh	T3-U2 W^*	T3-U2 M_{22}^*	T3-U2 M_{11}^*	T6-U3 w^*	T6-U3 M_{22}^*	T6-U3 M_{11}^*	T10-U4 w^*	T10-U4 M_{22}^*	T10-U4 M_{11}^*
2 × 2	0.421115	0.64790	1.33819	0.443104	1.62431	2.52722	0.246108	0.60215	1.16324
4 × 4	0.393999	1.01757	1.67013	0.348698	1.30423	1.98429	0.356469	1.05704	1.76663
8 × 8	0.305318	1.11745	1.58532	0.326564	0.86335	1.71994	0.365434	0.95047	1.78325
16 × 16	0.285607	1.05519	1.61422	0.358165	0.97179	1.80192	0.390331	1.02111	1.85543
24 × 24	0.309866	1.05211	1.68162	0.376441	0.99480	1.82813			
32 × 32	0.330657	1.00984	1.72183						
48 × 48	0.360440	0.96062	1.77377						
Ref. (Morley, 1962)	0.4080	1.08	1.91	0.4080	1.08	1.91	0.4080	1.08	1.91

Element mesh	*T3BL* (Taylor and Auricchio, 1993) W^*	*T3BL* M_{22}^*	*T3BL* M_{11}^*	*MIN6* w^*	*MIN6* M_{22}^*	*MIN6* M_{11}^*
2 × 2	0.537100	0.74915	1.44018	0.443109	1.62421	2.52671
4 × 4	0.420881	0.95544	1.72257	0.348478	1.30308	1.98405
8 × 8	0.415286	1.09045	1.89280	0.324182	0.83373	1.70398
16 × 16	0.413626	1.10028	1.91234	0.354328	0.93747	1.78247
24 × 24				0.373069	0.97850	1.81691
32 × 32	0.412734	1.09998	1.91781			
48 × 48						
64 × 64	0.412062	1.10022	1.91790			
Ref. (Morley, 1962)	0.4080	1.08	1.91	0.4080	1.08	1.91

Note: Displacement and moment at the centre with regular meshes, $L/h = 1{,}000$

Table XVIII.
Simply supported skew plate (SS1)

Element mesh	*9βQ4* (de Miranda and Ubertini, 2006) W^*	M_{22}^*	M_{11}^*
2 × 2			
4 × 4	0.501994	1.352235	2.056188
8 × 8	0.442198	1.079937	1.955570
16 × 16	0.430832	1.149342	1.964564
24 × 24			
32 × 32	0.424505	1.143222	1.953153
48 × 48			
Ref. (Morley, 1962)	0.4080	1.08	1.91

Element mesh	*Q4-U2* w^*	*Q4-U2* M_{22}^*	*Q4-U2* M_{11}^*	*Q9-U3* w^*	*Q9-U3* M_{22}^*	*Q9-U3* M_{11}^*	*Q16-U4* w^*	*Q16-U4* M_{22}^*	*Q16-U4* M_{11}^*
2 × 2	0.00087	0.0018	0.0048	0.15198	0.2596	0.5436	0.24947	0.7742	1.4298
4 × 4	0.00940	0.0222	0.0604	0.24245	0.5181	1.0542	0.32983	0.8966	1.7738
8 × 8	0.08101	0.1991	0.5320	0.31048	0.7569	1.5423	0.35493	0.9036	1.7595
16 × 16	0.20304	0.4738	1.1403	0.35670	0.9010	1.7574	0.37775	0.9730	1.8191
24 × 24	0.27309	0.6451	1.4369	0.37401	0.9595	1.8097			
32 × 32	0.31365	0.7544	1.5910						
48 × 48	0.35353	0.8802	1.7386						
Ref. (Morley, 1962)	0.4080	1.08	1.91	0.4080	1.08	1.91	0.4080	1.08	1.91

Note: Displacement and moment at the centre using a quadrilateral hybrid element (de Miranda and Ubertini, 2006) and linked-interpolation elements (Ribarić and Jelenić, 2012), $L/h = 1{,}000$

Table XIX.
Simply supported skew plate (SS1) under uniformly distributed load

Element mesh	T3-U2 d.o.f.	T3-U2 w_c^*	T3-U2 M_c^*	T6-U3 d.o.f.	T6-U3 w_c^*	T6-U3 M_c^*	T10-U4 d.o.f.	T10-U4 w_c^*	T10-U4 M_c^*
6	12	0.401654	4.7169	42	0.415578	5.44937	72	0.415956	5.1564
24	42	0.411726	5.0351	156	0.415978	5.23677	270	0.416000	5.1567
96	156	0.414989	5.1280	600	0.415999	5.17735	1044	0.415991	5.1573
384	600	0.415747	5.1497						
Ref. (de Miranda and Ubertini, 2006)		0.415994	5.1563		0.415994	5.1563		0.415994	5.1563

Element mesh	*T3BL* (Taylor and Auricchio, 1993) w^*	M_c^*
6	0.411627	4.72366
24	0.414296	5.02944
96	0.415555	5.12392
384	0.415891	5.14840
1,536	0.415971	5.15445
6,144	0.415989	5.15586
Ref. (de Miranda and Ubertini, 2006)	0.415994	5.1563

Note: Displacement and moment at the centre, $R/h = 5$

Table XX. Simply supported circular plate (SS1) with uniform load on meshes from Figure 21

Element mesh	T3-U2 d.o.f.	T3-U2 w_c^*	T3-U2 M_c^*	T6-U3 d.o.f.	T6-U3 w_c^*	T6-U3 M_c^*	T10-U4 d.o.f.	T10-U4 w_c^*	T10-U4 M_c^*
6	12	0.341539	3.7043	42	0.396171	5.5157	72	0.396469	5.1413
24	42	0.379082	4.6686	156	0.398321	5.2512	270	0.397956	5.1505
96	156	0.393800	5.0691	600	0.398257	5.1758	1,044	0.398176	5.1617
384	600	0.397745	5.1462						
Ref. (de Miranda and Ubertini, 2006)		0.398315	5.1563		0.398315	5.1563		0.398315	5.1563

Element mesh	*T3BL* (Taylor and Auricchio, 1993) w^*	M_c^*
6	0.394319	4.70841
24	0.396576	5.03098
96	0.397848	5.12424
384	0.398200	5.14859
1,536	0.398287	5.15448
6,144	0.398308	5.15586
Ref. (de Miranda and Ubertini, 2006)	0.398315	5.1563

Note: Displacement and moment at the centre, $R/h = 50$

Table XXI. Simply supported circular plate (SS1) with uniform load on meshes from Figure 21

are identical to the problem from Figure 21. For the thin plate situation ($R/h = 50$) the exact solution for the central displacement is known (de Miranda and Ubertini, 2006), while the bending moment at the centre has a singularity:

$$\text{With}: \quad w_c^* = \frac{w_c}{P}\frac{100D}{4R^2}, \quad M_c^* = \frac{M_c}{P} \ \text{(at closest Gauss point)}$$

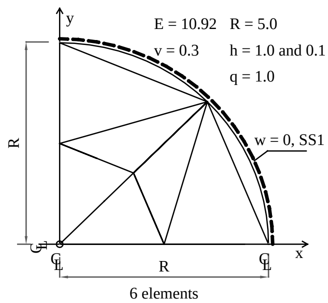

Note: Three meshes used in analysis in Tables XX-XXII

Figure 21. A simply supported (SS1) 1/4 of the circular plate under uniform load

Element mesh	*9βQ4* (de Miranda and Ubertini, 2006) w_c^*	M_c^*	*Q4-U2* w_c^*	M_c^*	*Q9-U3* w_c^*	M_c^*	*Q16-U4* w_c^*	M_c^*
3	0.2692074	5.10642	0.3486007	3.85988	0.3904531	5.10265	0.397474	5.1484
12	0.3959145	5.14593	0.3828163	4.82198	0.3981520	5.17865	0.398265	5.1553
48	0.3977919	5.16070	0.3968067	5.12375	0.3982781	5.16337		
192	0.3981935	5.15773	0.3981513	5.15283				
768	0.3982894	5.15668						
Ref. (de Miranda and Ubertini, 2006)	0.398315	5.1563	0.398315	5.1563	0.398315	5.1563	0.398315	5.1563

Note: Displacement and moment at the centre, $R/h = 50$, using a quadrilateral hybrid element (de Miranda and Ubertini, 2006) and quadrilateral linked-interpolation elements (Ribarić and Jelenić, 2012)

Table XXII. Simply supported circular plate (SS1) with uniform load

Element mesh	d.o.f.	*T3-U2* w_c^*	M_c^*	d.o.f.	*T6-U3* w_c^*	M_c^*	d.o.f.	*T10-U4* w_c^*	M_c^*
6	12	0.904743	0.101126	42	1.235808	0.279935	72	1.256633	0.366285
24	42	1.125456	0.184045	156	1.258859	0.348196	270	1.262771	0.431803
96	156	1.230098	0.273531	600	1.263289	0.420456	1,044	1.264680	0.503816
384	600	1.257735	0.352032						
Ref. (de Miranda and Ubertini, 2006)		1.262528	∞		1.262528	∞		1.262528	∞

Note: Displacement and moment at the centre, $R/h = 50$

Table XXIII. Simply supported circular plate (SS1) with the point load at the centre

7. Conclusions

A displacement-based linked-interpolation concept for designing triangular Mindlin plate finite elements has been presented and numerically verified. The idea has been presented in its general form applicable to triangular elements of any order, but the numerical results have been provided for the first three elements of the family, i.e. the three-, six- and ten-node plate elements. In all the elements from the family the leading design principle is borrowed from the underlying family of Timoshenko beam elements. Thus, the original shear strain condition of a certain order imposed along the beam has been applied to the plate element edges leading to 2D generalisation of the beam-type linked interpolation for the displacement field, whereby, both nodal rotations contribute to the element out-of-plane displacements.

It has been shown that, for the elements with more than two nodes per side, additional internal degrees of freedom are required in order to provide full polynomial expansion of certain order. The number of these degrees of freedom is linearly growing by one, beginning with no internal degrees of freedom for the lowest-order three-node member of the family. The elements developed in this way give exact result for cylindrical bending of a corresponding order, e.g. quadratic distribution of the out-of-plane displacements for the three-node elements, cubic for the six-node elements and so on. However, in contrast to beams, the developed elements still suffer from shear locking for very coarse meshes of the lowest-order element types. In particular, the results for the thin clamped square plate have shown that the lowest-order triangular linked-interpolation element (*T3-U2*) may suffer from considerable shear locking and cannot be considered as reliable, while a certain amount of locking is also present in *T6-U3*.

Performance of these elements has been numerically analysed and it has been found out, that they perform well for a number of standard benchmark tests. It has to be stressed, however, that the well-known Morley's skewed plate example again turns out to be rather demanding confirming the earlier conclusion for the quadrilateral displacement-based linked-interpolation elements that, for this test, the proposed design principle cannot compete with the mixed-type approach. Otherwise, the higher-order members of the element family turn out to be successful when compared to the lower-order elements from literature for the problems with the same total number of the degrees of freedom.

Nevertheless, the lowest-order element with three nodes is the one with the greatest practical interest for its versatility. Work is under way to improve it by adding a number of internal bubble functions in the displacement and rotation fields associated with corresponding bubble parameters (Ribarić, 2012), which are specifically chosen to satisfy the basic patch test necessary for the element consistency and enable a softer response in the bench-mark test examples.

References

Auricchio, F. and Lovadina, C. (2001), "Analysis of kinematic linked interpolation methods for Reissner-Mindlin plate problem", *Computer Methods in Applied Mechanics and Engineering*, Vol. 190, pp. 2465-2482.

Auricchio, F. and Taylor, R.L. (1993), "A new family of quadrilateral thick plate finite elements based on linked interpolation", Report No. UCB/SEMM-93/10, Department of Civil Engineering, University of California at Berkeley, Berkeley.

Auricchio, F. and Taylor, R.L. (1994), "A shear deformable plate element with an exact thin limit", *Computer Methods in Applied Mechanics and Engineering*, Vol. 118, pp. 393-412.

Auricchio, F. and Taylor, R.L. (1995), "A triangular thick plate finite element with an exact thin limit", *Finite Elements in Analysis and Design*, Vol. 19, pp. 57-68.

Babuška, I. and Scapolla, T. (1989), "Benchmark computation and performance evaluation for a rhombic plate bending problem", *International Journal for Numerical Methods in Engineering*, Vol. 28, pp. 155-179.

Bathe, K.-J. (1989), *Finite Element Procedures*, Prentice-Hall, Englewood Cliffs, NJ.

Bathe, K.-J., Brezzi, F. and Choo, S.W. (1989), "The MITC7 and MITC9 plate bending elements", *Computers & Structures*, Vol. 32, pp. 797-814.

Chen, W.J. (2006), "Enhanced patch test of finite element methods", *Science in China, Series G: Physics, Mechanics & Astronomy*, Vol. 49 No. 2, pp. 213-227.

Chen, W.J. and Cheung, Y.K. (2000), "Refined quadrilateral element based on Mindlin-Reissner plate theory", *International Journal for Numerical Methods in Engineering*, Vol. 47, pp. 605-627.

Chen, W.J. and Cheung, Y.K. (2001), "Refined 9-dof triangular Mindlin plate elements", *International Journal for Numerical Methods in Engineering*, Vol. 51, pp. 1259-1281.

Chen, W.J. and Cheung, Y.K. (2005), "Refined discrete quadrilateral degenerated shell element by using Timoshenko's beam function", *International Journal for Numerical Methods in Engineering*, Vol. 63, pp. 1203-1227.

Chen, W.J., Wang, J.Z. and Zhao, J. (2009), "Functions for patch test in finite element analysis of the Mindlin plate and the thin cylindrical shell", *Science in China, Series G: Physics, Mechanics & Astronomy*, Vol. 52 No. 5, pp. 762-767.

Chinosi, C. and Lovadina, F. (1995), "Numerical analysis of some mixed finite element methods for Reissner-Mindlin plate", *Computational Mechanics*, Vol. 16, pp. 36-44.

Crisfield, M.A. (1986), *Finite Elements and Solution Procedures for Structural Analysis*, Pineridge Press, Swansea.

de Miranda, S. and Ubertini, F. (2006), "A simple hybrid stress element for shear deformable plates", *International Journal for Numerical Methods in Engineering*, Vol. 65, pp. 808-833.

Hughes, T.J.R. (2000), *The Finite Element Method: Linear Static and Dynamic Finite Element Analysis*, Dover Publications Inc., Mineola, NY.

Hughes, T.J.R. and Tezduyar, T.E. (1981), "Finite elements based upon Mindlin plate theory with particular reference to the four-node bilinear isoparametric element", *Journal of Applied Mechanics*, Vol. 48, pp. 587-596.

Ibrahimbegović, A. (1993), "Quadrilateral finite-elements for analysis of thick and thin plates", *Computer Methods in Applied Mechanics and Engineering*, Vol. 110, pp. 195-209.

Jelenić, G. and Papa, E. (2011), "Exact solution of 3D Timoshenko beam problem using linked interpolation of arbitrary order", *Archive of Applied Mechanics*, Vol. 18, pp. 171-183.

Kim, D.-N. and Bathe, K.-J. (2009), "A triangular six-node shell element", *Computers & Structures*, Vol. 87, pp. 1451-1460.

Lee, P.-S. and Bathe, K.-J. (2004), "Development of MITC isotropic triangular shell elements", *Computers & Structures*, Vol. 82, pp. 945-962.

Liu, Y.J. and Riggs, H.R. (2005), "The MIN-N family of pure-displacement, triangular, Mindlin plate elements", *Structural Engineering and Mechanics*, Vol. 19, pp. 297-320.

Morley, L.S.D. (1962), "Bending of simply supported rhombic plate under uniform normal loading", *Quarterly Journal of Mechanics and Applied Mathematics*, Vol. 15, pp. 413-426.

Mukherjee, S., Reddy, J.N. and Krishnamoorthy, C.S. (2001), "Convergence properties and derivative extraction of the superconvergent Timoshenko beam finite element", *Computer Methods in Applied Mechanics and Engineering*, Vol. 190, pp. 3475-3500.

Naumenko, K., Altenbach, J., Altenbach, H. and Naumenko, V.K. (2001), "Closed and approximate analytical solution for rectangular Mindlin plates", *Acta Mechanica*, Vol. 147, pp. 153-172.

Przemieniecki, J. (1968), *Theory of Matrix Structural Analysis*, McGraw-Hill, New York, NY.

Rakowski, J. (1990), "The interpretation of the shear locking in beam elements", *Computers & Structures*, Vol. 37, pp. 769-776.

Reddy, J.N. (1997), "On locking-free shear deformable beam finite elements", *Computer Methods in Applied Mechanics and Engineering*, Vol. 149, pp. 113-132.

Ribarić, D. (2012), "Higher-order linked interpolation in moderately thick plate and facet shell finite elements", doctoral thesis (in preparation), University of Rijeka, Rijeka.

Ribarić, D. and Jelenić, G. (2012), "Higher-order linked interpolation in quadrilateral thick plate finite elements", *Finite Elements in Analysis and Design*, Vol. 51, pp. 67-80.

Simo, J.C. and Rifai, M.S. (1990), "A class of mixed assumed-strain methods and the method of incompatible modes", *International Journal for Numerical Methods in Engineering*, Vol. 29, pp. 1595-1638.

Taylor, R.L. and Auricchio, F. (1993), "Linked interpolation for Reissner-Mindlin plate elements: part II – a simple triangle", *International Journal for Numerical Methods in Engineering*, Vol. 36, pp. 3057-3066.

Taylor, R.L. and Govindjee, S. (2002), "A quadratic linked plate element with an exact thin plate limit", Report No. UCB/SEMM-2002/10, Department of Civil and Environmental Engineering, University of California at Berkeley, Berkeley, CA.

Tessler, A. (1989), "A C0-anisoparametric three-node shallow shell element for general shell analysis", Report MTL TR 89-72, US Army Materials Technology Laboratory, Watertown, MA.

Tessler, A. and Dong, S.B. (1981), "On a hierarchy of conforming Timoshenko beam elements", *Computers & Structures*, Vol. 14, pp. 335-344.

Tessler, A. and Hughes, T.J.R. (1985), "A three-node Mindlin plate element with improved transverse shear", *Computer Methods in Applied Mechanics and Engineering*, Vol. 50, pp. 71-101.

Xu, Z., Zienkiewicz, O.C. and Zeng, L.F. (1994), "Linked interpolation for Reissner-Mindlin plate elements: part III – an alternative quadrilateral", *International Journal for Numerical Methods in Engineering*, Vol. 37, pp. 1437-1443.

Yunhua, L. (1998), "Explanation and elimination of shear locking and membrane locking with field consistence approach", *Computer Methods in Applied Mechanics and Engineering*, Vol. 162, pp. 249-269.

Zhu, Z. (1992), "A thick-thin triangular plate element", *International Journal for Numerical Methods in Engineering*, Vol. 33, pp. 963-973.

Zienkiewicz, O.C. and Taylor, R.L. (2005), *The Finite Element Method for Solid and Structural Mechanics*, Elsevier Butterworth-Heinemann, Oxford.

Zienkiewicz, O.C., Taylor, R.L. and Zhu, J.Z. (2005), *The Finite Element Method: Its Basis and Fundamentals*, Elsevier Butterworth-Heinemann, Oxford.

Zienkiewicz, O.C., Xu, Z., Zeng, L.F., Samuelsson, A. and Wiberg, N.E. (1993), "Linked interpolation for Reissner-Mindlin plate elements: part I – a simple quadrilateral", *International Journal for Numerical Methods in Engineering*, Vol. 36, pp. 3043-3056.

About the authors

Dragan Ribarić is a Senior Lecturer of mechanics at the Faculty of Civil Engineering, University of Rijeka. He is a doctoral candidate and a Teacher for a number of undergraduate courses in engineering and structural mechanics. His research interests are plate and shell structures, structural analysis, and finite element design.

Gordan Jelenić is an Associate Professor of mechanics at the Faculty of Civil Engineering, University of Rijeka. Between 1990 and 1993, he was a Research Assistant in the Faculty of Civil and Geodetic Engineering, University of Ljubljana, between 1994 and 1998 he was a Research Associate and between 1999 and 2004 a Research Fellow in the Department of Aeronautics, Imperial College London. He teaches a number of undergraduate and postgraduate courses in mechanics of rigid and deformable bodies and is Head of Chair of Engineering Mechanics. His main research interests lie in the areas of non-linear computational mechanics, finite element method, and numerical integration in dynamics. Gordan Jelenić is the corresponding author and can be contacted at: gordan@gradri.hr